Materials Science and Engineering C 69 (2016) 905–913

Contents lists available at ScienceDirect

Materials Science and Engineering C

journal homepage: www.elsevier.com/locate/msec

Physicochemical characterization of three fiber-reinforced epoxide-based composites for dental applications

Anderson J. Bonon [a], Marcus Weck [b], Estevam A. Bonfante [c,*], Paulo G. Coelho [d,e]

[a] Faculdade de Engenharia Química, Universidade Estadual de Campinas, Av. Albert Einstein, 500, Campinas, SP CEP 13083-852, Brazil
[b] Molecular Design Institute and Department of Chemistry, New York University, New York, NY 10003, United States
[c] Department of Prosthodontics and Periodontology, University of Sao Paulo - Bauru School of Dentistry, Bauru, Brazil
[d] Department of Biomaterials and Biomimetics, New York University College of Dentistry, New York, NY, USA
[e] Hansjörg Wyss Department of Plastic Surgery, New York University School of Medicine, New York, NY, USA

ARTICLE INFO

Article history:
Received 7 July 2015
Received in revised form 26 June 2016
Accepted 4 July 2016
Available online 05 July 2016

Keywords:
Fiber-reinforced composites
BPA
Degradation
Physicochemical

ABSTRACT

Fiber-reinforced composite (FRC) biomedical materials are in contact with living tissues arising biocompatibility questions regarding their chemical composition. The hazards of materials such as Bisphenol A (BPA), phthalate and other monomers and composites present in FRC have been rationalized due to its potential toxicity since its detection in food, blood, and saliva. This study characterized the physicochemical properties and degradation profiles of three different epoxide-based materials intended for restorative dental applications. Characterization was accomplished by several methods including FTIR, Raman, Brunauer–Emmett–Teller (BET) Analysis, X-ray fluorescence spectroscopy, and degradation experiments. Physicochemical characterization revealed that although materials presented similar chemical composition, variations between them were more largely accounted by the different phase distribution than chemical composition.

1. Introduction

One of the most important classes of polymeric materials is epoxy resin. Its wide applicability is due to its combination of properties such as excellent chemical and corrosion resistance, high tensile strength, dimensional stability, low modulus of elasticity, along with its easy processing and manufacturing. An important factor that increases the scope of the epoxy resin market is its good compatibility with a variety of copolymers (e.g., poly(ε-caprolactone), poly(dimethylsiloxane), poly(amide)s and dendrimers) as well as composites (e.g., metallic oxides, carbon black, natural and glass fiber), significantly increasing and tuning the properties of the final material [1–4]. The most common epoxy resin is the polyether diglycidyl ether bisphenol A resin (DGEBA) [5]. In order to obtain a cross-link polymer and reduce the gelation time at plausible process conditions, dicyandiamide (DCD) is prevalently used as curing agent. Imidazole is often incorporated to the formulation to alter the glass transition temperature [6].

The filling of poly (methyl methacrylate) (PMMA) into the pores of graphene aerogel has been described where an increase in graphene loading lead to increases in thermal and electrical conductivity as well as in microhardness [7]. By methods such as aqueous phase exfoliation, high-yield graphene nanosheets have been developed with substantial increase in surface area and improvement in thermal stability [8]. When prepared by thermal reduction of graphite oxide and modified with stearic acid to enhance its lipophilicity, graphene composites have shown improved tensile resistance with enhanced dispersion of graphene in a low density polyethylene matrix [9]. Also, the incorporation of magnetite nanoparticles in a sulfonated polyaniline matrix has been characterized showing an additional crystalline order and improved conductivity. [10] Lastly, a comprehensive review has elaborated on a variety of synthesis strategies of the next generation TiO_2-based hybrid photocatalysts, under attention due to their excellent physicochemical properties, produced in combination with polymers and carbon nanomaterials [11].

When reinforced with fibers, epoxide based composites can attain high stiffness-to-weight and strength-to-weight ratios, properties of significant importance in biomedical applications such as artificial tendons, ligaments, intervertebral disks, and hip stems [12]. In dentistry, common uses include fiber-reinforced prefabricated posts that are cemented into root canals with widely reported success rates [13,14], orthodontic brackets, and, more recently, restorative materials [13]. Since fiber-reinforced composites (FRC) composition can be tailored to match the mechanical properties of the tissues they replace, its use has gained interest as an alternative to metals and ceramics in full-mouth reconstructions. Simulations have shown that for implant-supported prostheses, all stresses transmitted to peri-implant tissues

* Corresponding author at: Department of Prosthodontics, University of São Paulo, Al Otávio Pinheiro Brisola 9-75, Bauru, SP 17.012-901, Brazil.
E-mail address: estevamab@gmail.com (E.A. Bonfante).

http://dx.doi.org/10.1016/j.msec.2016.07.002
0928-4931/

are significantly greater for metal ceramics compared to FRC prostheses [15].

One aspect that concerns the biomedical use of FRC is that the unreacted compounds remain trapped in the polymeric network, and depending on the environmental conditions and the stress the materials undergo, these compounds may be released to the surrounding environment. Currently, many polymeric formulations intended for biomedical applications contain BPA that is used as a catalyst in the reaction between epoxide and amine groups where all the BPA added to the reaction is not necessarily covalently bonded to the polymer network and therefore may leach from the bulk material under service to variable amounts depending on the overall polymer physicochemical characteristics.

Due to the extremely high global demand for epoxy resin, poly(carbonate), poly(vinyl chloride)s (PVC), poly(acrylate), and poly(sulfone), >2.7 million tons of BPA are produced each year. The majority of these materials are used in food containers, plastic packing, coating resin for metal cans, water pipes, bottles, storage containers and dental sealants [16–18]. In the last decade, a significant increase in the investigation of the hazards of materials such as BPA, phthalate and other monomers and composites have been rationalized due to its potential toxicity since it has been previously detected in food, blood, and saliva. For instance, the range of 1–6 ppb of related compounds were found in samples of urine in over 93% of the North American population [19–22]. To date there is a controversy regarding what the toxic dosage of BPA or its cumulative effect on different organs and systems are.

A recent report by Zeliger [23] has suggested a potential relationship between lipophilic chemicals (which includes BPA among a multitude of other chemical byproducts) and neurologic diseases originating mainly from polluted air and water as well as contaminated food [23]. In addition to BPA, other classes of lipophilic compounds such as dioxins, organochlorine pesticides, furans, poly aromatic hydrocarbons, low molecular weight hydrocarbons (e.g., benzene, toluene, xylenes, gasoline, etc.), and phthalates have all been demonstrated to penetrate the blood-brain barrier [24]. These lipophilic compounds when combined have been regarded as hazardous even at low concentration levels relative to individual components in higher concentrations [23]. To date, data regarding BPA exposure quantity has been generated by the US Environmental Protection Agency (EPA). However, no consensus exist in the literature regarding the presence of BPA on a variety of dental materials, as dental materials related exposure has been shown to be transient and can potentially be controlled through adequate material processing and clinical procedures [25].

Considering that the use of FRC prostheses in contact with living tissues may raise biocompatibility questions regarding its chemical composition and stability, this study aimed to characterize the physicochemical properties and degradation profiles of three different epoxide-based materials intended for restorative dental applications as a first step prior to in vivo and clinical studies.

2. Materials and methods

2.1. Materials

Dimethyl sulfoxide (DMSO)-*d6* 99.9% (CIL) was used as-received. The Adsorption Buffer containing the same ions present in the saliva (without the enzymes) was provided by the laboratory of Basic Science and Craniofacial Biology of the New York University College of Dentistry, and it was prepared as previously described [26,27]. Three different FRC experimental materials were tested as received from the manufacturer. Two of the materials presented the polymeric components with different amounts of glass fiber content (materials A and B), whereas a third material (material C) presented a polymeric structure different than A and B. All materials were provided in disks of 4 in (10.16 cm) diameter by 1 in (2.54 cm) height.

2.2. Sample cutting

The samples were cut using a MICRO-Bandsaw MBS/E with a steel super fine tooth blade #85 in blocks of approximately 5 × 5 × 5 mm.

2.3. Cryogenic grounding

The solid samples were ground to a fine powder using a Cryomill MM 400 (Retsch, Germany). The samples were pre-cooled with liquid nitrogen for 5 min in the grinding container. The grinding time was set to 3 min at 30 Hz. During the process, samples were kept at temperature with liquid nitrogen.

2.4. Thermal gravimetric analyses (TGA)

The samples were analyzed using a TGA (PerkinElmer, Pyris 1) from 30 °C to 800 °C at 10 °C/min, and a N_2 flow at 50 mL/min. The total run time per sample was 78 min. The samples were analyzed in triplicate.

2.5. Differential scanning calorimetry (DSC)

The samples were analyzed using a DSC1 (METTLER TOLEDO). Temperature program: from 25 to 250 °C, at 10 °C/min, 250 °C for 3 min; from 250 to 25 °C at −10 °C/min; 25 °C, 25 °C for 3 min; from 25 to 250, at 10 °C/min, with 50 mL/min of N_2 flow. The glass transition temperature was determined in the middle point of the crossing tangents.

2.6. Scanning electron microscopy (SEM)

The samples were coated with gold with a system Sputter Coater POLARON (VG Microtech - Uckfield, England; Model: SC7620). The scanning electron micrographs were obtained by the Leica-Zeiss LEO 440i, with 15 kV of acceleration and current of 50 pA. Typically, the images were collected with a magnification of 500 and 1000 times.

2.7. Particle size distribution analysis

Two different techniques were used for particle size distribution analysis: laser diffraction and digital dynamic imaging. The laser diffraction was carried out using a HORIBA LA-950. Analysis was done in triplicate by sampling and measuring (totaling $n = 9$ measurements for each sample); ethanol was used as the dispersion medium without any surfactant addition. The transmittance utilized was between 95% and 98%, with ultrasonic probe off. The complex refractive index, composed of real and imaginary parts (1.54–0.10 i for the epoxy resin and 1.361 for ethanol) was used for deconvolution of the diffraction patterns and data process, based on the full Mie theory (software HORIBA LA-950). The Portable FlowCAM VS·I ("Fluid Imaging Technologies") instrument was used for the dynamic image analysis. Ethanol was used as dispersion medium, with 10× and 20× optical amplification lens and 300 μm flowcell. Images of the samples were introduced in the size distribution graph obtained by laser diffraction.

2.8. Fourier transformed infra-red (FTIR) analysis

The samples were analyzed using a FTIR spectrometer (Thermo Scientific model Nicolet 6700) carried out in the Attenuated Total Reflectance (ATR) mode, with a scanning range from 4000 to 600 cm^{-1} at a speed of 4 cm^{-1}/s, and with an average of 128 measurements in the final spectrum.

2.9. Raman spectroscopy analysis

The samples were analyzed using a Raman spectrometer (Horiba Scientific model XploRA™ PLUS) with a scanning range from 4000 to

200 cm^{-1}. The final spectrum is an average of 128 measurements, obtained with a laser of 532 nm.

2.10. The Brunauer–Emmett–Teller (BET) analysis

Adsorption characterization was performed using a Quantachrome Autosorb (Quantachrome Instruments, Boynton Beach, FL USA) with N_2 as the adsorbate at liquid nitrogen temperature (~77 K). Prior to measuring the surface area, the samples were outgassed at 150 °C for ~3 h. The surface area was calculated utilizing the multipoint Brunauer-Emmett-Teller (BET) method, the nitrogen adsorption isotherms by assuming the area of a nitrogen molecule to be 16.2 $Å^2$, as well as by the adsorption data from the partial pressure change ranging from $0.05 < P/P_0 < 0.35$, using ASORB2PC v1.05 software (Quantachrome Instruments, Boynton Beach, FL, USA). The measuring of surface area of the powder constituted of approximately 375 mg of dried and degassed particulate.

2.11. Determination of Ti, P and Si content by inductively coupled plasma optical emission spectroscopy (ICP-OES)

For trace elemental determination, the sample was weighed into a suitable digestion flask. For percent level determinations, an amount of sample was weighed such that the expected final preparation contained approx. 10–50 ppm of the element(s) of interest (i.e. Ti, Si and P). An additional digestion flask was prepared for a blank. The digestion acid (e.g., nitric, perchloric, or sulfuric acid) was added and each flask was heated on a suitable digestion rack until samples were fully digested.

Measurements were carried out on an ICP Perkin Elmer ICP Optima 7399DV calibrated using the standard solutions. The content for each element in the sample was calculated as follows:

$$(E)ppm = \frac{response\ (E) \times dilitionfactor \times Std_E ppm}{response(Std_E) \times sampleweight\ (g)}$$

where (E) *ppm* = ppm of the individual element in the sample; *Response* (E) = optical emission of the individual element in the sample; *dilution factor* = 5.0 mL plus volume of digestion acid added to each sample; Std_E *ppm* = ppm of the respective individual element added to the reagent spike preparation; *Response* (Std_E) = optical emission of the individual element in the reagent spike preparation; *Sample weight* (g) = weight of the sample, in grams in used in the samples preparation.

2.12. Carbon, hydrogen, and nitrogen (CHN) determination

For CHN determination, approximately 1.5 mg of sample was weighed into a tin capsule using the Cahn Electrobalance. The capsule was sealed, and reweighed to determine the final sample weight. The sample was then placed into the Perkin-Elmer Model 2400 CHN Analyzer carousel. Analysis was carried out under high purity Helium and oxygen (99.9%) as combustion gas, at 950 °C. The instrument was calibrated using a 141d Acetanilide, NIST standard.

2.13. X-ray fluorescence spectroscopy

The inorganic characterization were carried out on an Energy Dispersive X-Ray Fluorescence (EDXRF) Bruker S2 Ranger, equipped with a 50 W Rhodium X-ray tube and X-Flash® SDD detector. All measurements were performed under Helium.

2.14. Degradation experiments

The extractions were carried out by adding 1 g of powdered sample in 40 ml of solvent (methanol or adsorption buffer). The mixtures were magnetically agitated for two and 15 days in methanol, 28 and 56 days for adsorption buffer extraction. The extracts were concentrated for ^{1}H NMR analysis. To determine the leaching amount of BPA present in the samples, leaching experiments were performed in methanol, adapted from Perrin et al. in 2006 [28].

2.15. Bisphenol a determination by ^{1}H NMR

^{1}H NMR spectra of the concentrated samples were acquired at 25 °C on a Bruker AV600 spectrometer operating at 600 MHz, using deuterated dimethyl-sulphoxide (DMSO-*d6*) as a solvent and naphthalene as an internal standard. Determination of Bisphenol A (BPA) leaching was calculated by the formula:

$$\%BPA = \left(\frac{W_N}{W_S}\frac{I_a}{I_c}\right) \times 178$$

where: W_N is the weight of naphthalene; W_S is the sample amount; I_c is the integral of the naphthalene protons ($\delta = 7.91$ ppm); I_a is the integral of the bisphenol A protons ($\delta = 6.98$ ppm); and 178 is the (molecular weight of bisphenol A / molecular weight of naphthalene) × 100. The results were expressed in terms of total mass percentage (%), parts per million (mg/kg, ppm) and organic percentage (%Org) which is the amount of BPA leaching in relation to the organic fraction, obtained by TGA.

2.16. Dicyandiamide leaching by ^{1}H NMR

^{1}H NMR spectra of the concentrated samples were acquired at 25 °C on a Bruker AV600 spectrometer operating at 600 MHz, using DMSO-*d6* as a solvent and naphthalene as an internal standard. Determination of Dicyandiamide (DCA) leaching was calculated by the formula:

$$\%DCA = \left(\frac{W_N}{W_S}\frac{I_a}{I_c}\right) \times 65.6$$

where: W_N is the weight of naphthalene; W_S is the sample amount; I_c is the integral of naphthalene protons ($\delta = 7.91$ ppm); I_a is the integral of dicyandiamide protons ($\delta = 6.52$ ppm); and 65.6 is the (molecular weight dicyandiamide / molecular weight naphthalene) × 100. The results were expressed in terms of total mass percentage (%), parts per million (mg/kg, ppm) and organic percentage (%Org), which is the amount of DCA leaching in relation to the organic fraction, obtained by TGA.

3. Results and discussion

The elemental characterization of the samples for carbon, hydrogen, nitrogen and phosphorus are show in percentages in the Table 1. The first thermal characterization of the material performed by thermogravimetric analysis (TGA) (Fig. 1) were used to evaluate the thermal stability and determination of the organic and inorganic content, as summarized in Table 2. The thermal gravimetric analysis showed that sample A, B and C were remarkably stable over the tested temperature range especially since dental applications usually remain at body temperature for most of its service life. All samples presented an initial decomposition temperature onset at 400 °C despite the different inorganic/organic ratios observed between samples. Organic fraction was

Table 1
Elemental analysis, in mass percentage, of the samples A, B and C.

Sample	C (%)	H (%)	N (%)	P (%)
A	33.01	3.06	0.71	0.01
B	30.11	2.56	0.7	0.036
C	26.43	2.54	1.09	0.13

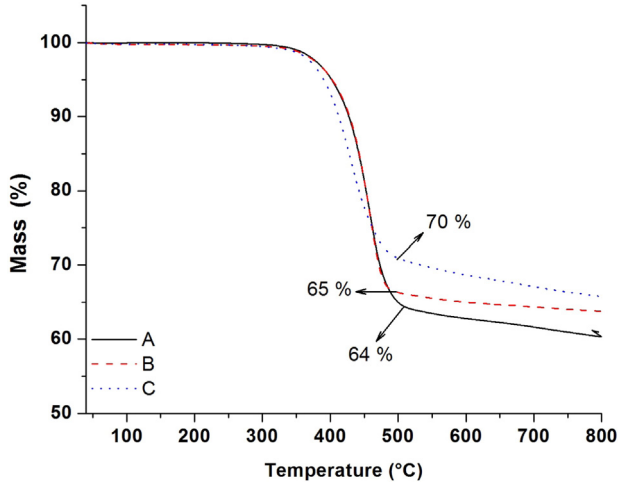

Fig. 1. Thermogram of samples A, B and C, average of triplicate measurements.

calculated based on the percentage of material decomposed up to 500 °C, where a plateau is observed. The derivative thermogravimetric (DTG) shows the only mass loss observed was the material decomposition (TGA and DTG data for each material is presented in Fig. S1)·The organic contents observed by TGA are in direct agreement with the elemental analyses for all three samples.

X-ray fluorescence depicted the main constituents of the inorganic fraction for all samples mainly comprised oxides of silicon, aluminum, calcium, iron, strontium and titanium (Table 3). Given that it was disclosed that the inorganic content of all materials was glass fiber, direct inferences of the different oxides (SiO_2/Al_2O_3/CaO/Fe_2O_3/SrO) with a ratio of 1/0.2/0.6/0.01/0.005 was the same for all the three samples tested. Such result indicates that similar glass fiber was used in all materials. In fact, the SiO_2/Al_2O_3/CaO ratio is similar to a ternary eutectic composition SiO_2–Al_2O_3–CaO that is described in the literature [29] as an environmentally friendly alternative to the largest used fluorine-borosilicate E-glass. Since only pure Si, Al and Ca oxides are involved in its processing, no toxic gas is formed during the manufacturing process besides its improved energy efficiency relative to its fluorine-borosilicate counterpart. The traces of SrO likely arose as a doping for CaO [30–32]. While Fe is a common impurity in alumina [33], the determined concentration in the samples indicates it was deliberately added to the glass crude mixture. The 1.5–4.6% of TiO_2 measured in the samples suggests that TiO_2 was added in the polymer mixture as a pigment as observed in many other dental materials applications. However, such common application of TiO_2 does not exclude the possibility of a portion of TiO_2 within the overall material composition to be present within the glass fiber.

To further characterize the thermal behavior of the materials; differential scanning calorimetry (DSC) was also performed (Fig. 2). Two heating procedures were performed. In the first heating, the samples were heated up to 250 °C in an attempt to provide energy to the system so unreacted products either react of are eliminated. Then, after the first heating cooling down to 25 °C, a second sample heating was performed to 250 °C in an attempt to determine the materials'characteristic physicochemical events. In the first heating, all materials showed an event around 100 °C, corresponding to humidity in the samples. Two endothermic events, at 112 °C and 130 °C, were observed for materials A and B. However, during the second heating, such endothermic events of the materials A and B were not observed. The absence of these endothermic events (at 112 °C and 130 °C) suggests these events are related to a chemical reaction, probably due to remaining unreacted reactants.

Table 2
TGA analyses, inorganic and organic content.

Sample	Inorganic (%)	Organic (%)	SD
A	64	36	3.0
B	65	35	3.5
C	70	30	1.5

Table 3
X-ray fluorescence analysis of the samples A, B and C.

Sample	SiO_2	Al_2O_3	CaO	Fe_2O_3	SrO	TiO_2
A	31.0	7.6	23.2	0.5	0.2	1.5
B	34.3	7.2	22.0	0.3	0.1	1.1
C	34.5	8.6	21.8	0.4	0.2	4.6

The transition glass temperature of materials A and B were determined as 101 °C and 103 °C, respectively, in the second heating procedure. Material C showed two T_gs, one at 97 °C and 182 °C. The higher T_g of the material C was observed in both heating procedures. The high glass transition temperatures are indicative of a high degree of polymerization and cross-linking. The samples' calorimetric profiles indicate a different chemical composition between material C relative to materials A and B. The individual DSC thermogram of the first and second heating are displayed in Figs. S2 and S3.

The particle size distribution for all samples presented a bimodal distribution by both analytical techniques (laser diffraction and image method). The median sizes by laser diffraction for material A were found to be 18.6 μm and 217.1 μm. 18.31 μm and 175.55 μm, and 14.31 μm and 93.6 μm are the bimodal median sizes for Materials B and C, respectively (Fig. 3). Fig. 3 depicts that particles with <50 μm are mostly glass fiber with low amounts of adhered polymer. The larger particles are mainly comprised by glass fibers within polymer matrix. Relative to material C, an increased amount of the smaller particles were observed for materials A and B. Such differences are likely accounted by differences in fiber content distribution between materials. Individual data are shown in Fig. S4.

The images of the particle obtained by SEM (Fig. 4) of the powdered materials shows the larger particles (>100 μm) are mainly polymer fragments, whereas the smaller portion of the particles are fragments of glass fiber, as observed in dynamic image analysis. More SEM images of the samples are available in the supplementary material Figs. S5, S6 and S7.

To determine the chemical identity of the polymeric materials with the presence of the glass fiber as composite, the samples were characterized by FTIR. The characteristic wavenumbers of diglycidyl ether bisphenol A resin and glass fiber were readily observed for the three samples (Fig. 5).

Due to the large amount of glass fiber in the materials, Raman spectroscopy counterproof was performed to further confirm the organic groups initially detected the infrared spectroscopy. The FT-IR and FT-Raman spectrum for each sample is presented in Fig. 4. From 1000 to 2500 cm^{-1}, a large increase is observed in the base line due to the scattering of the laser beam by the glass fiber. Despite such setback, a sharp band at 1600 cm^{-1} characteristic of the C–C stretching was easily identified. An exception, however, was encountered when the FTIR and Raman spectra were compared for material C, where the C–H stretching of the methyl and methylene groups at 2965 cm^{-1} and 2926 cm^{-1}, respectively, were possibly not detected due to the lower amount of organic fraction in the sample, as determinate by TGA. Comparison of the vibration patterns of the C=C bond stretching in the aromatic ring (1600 cm^{-1}) and C–C (1508 cm^{-1}) aromatic bond stretching, strongly indicates that the polymer present in all tested samples is diglycidyl ether bisphenol. The broad band at 1000 cm^{-1} is assigned to the oxygen-silicon bond in the Si–O–Si group of the glass fiber used as composite, and the Si-OH bending band was likely the one detected 823 cm^{-1}. When the FTIR and Raman spectra of the materials are evaluated in tandem, all materials presented the same organic groups at different relative intensities especially when those related to non-dissociative symmetrical groups were concerned such as the stretching of the

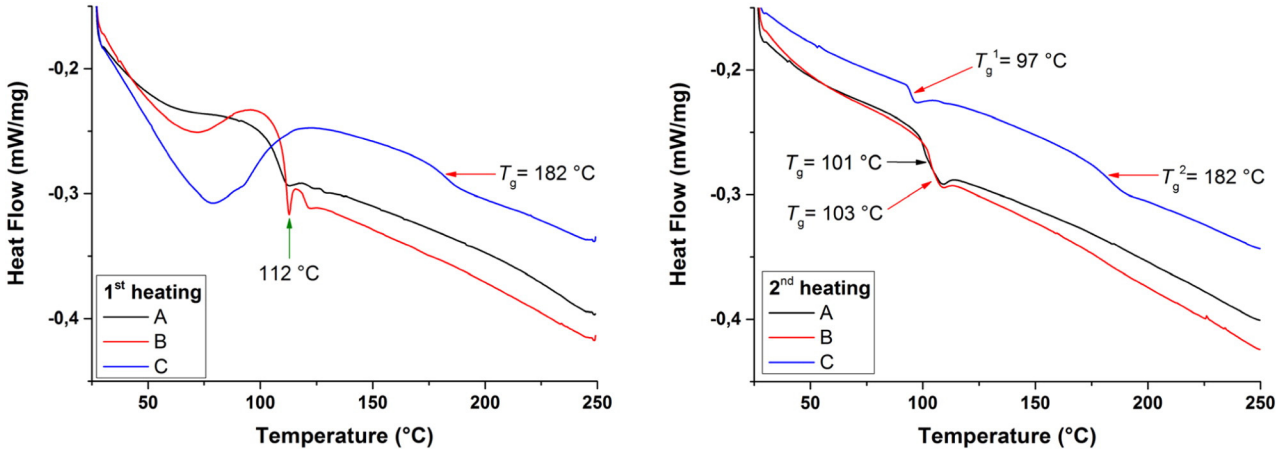

Fig. 2. DSC curves of the first and second heating of the materials A, B and C.

aromatic C–H. The symmetric stretching of the aromatic C–H band was identified at 3060 cm^{-1} of Raman shift for all the materials [34]. The stretch of C–OH, for a tertiary alcohol (1180 cm^{-1}), asymmetric (1240 cm^{-1}) and symmetric (1110 cm^{-1}) stretches of the C–O bond for an aryl-alkyl ether are present in materials A and B. Whereas in material C, only the C–O bond stretch for an alkyl ether (1140 cm^{-1}) was found, further indicating a compositional difference between materials C relative to materials A and B observed in our DSC results. The individual FTIR and Raman spectra are presented in Figs. S8 and S9. Table 4 summarizes the observed bands and its correspondent vibrational event.

To address potential biocompatibility differences between materials, the unreacted organic amount within the different materials were quantified. Our extractable BPA determination was carried out using methanol following the method proposed in 2006 by Perrin et al. [28]. The results for total leached BPA in methanol extraction are displayed in Fig. 7, and spectral analyses depicted undetectable leaching of DCA. Following the same experimental procedure using adsorption buffer for 28 days showed undetectable amounts of BPA were observed along with leached DCA at different degrees as presented in Fig. 8. An example of ^{1}H NMR spectrum for BPA and DCA extraction is shown on the Figs. S10 and S11, respectively. Yet, it is important to remember that whereas the safe reference dose for humans has been established at 50 μg/kg/day, the actual extent and exposure route of humans to BPA is still under debate [35].

The methanol extraction in two and 15 days show that there is no significant difference in BPA leaching (Fig. 7). This experiment demonstrates that the method applied for determination of total BPA leaching in two days in methanol medium is sufficient, as demonstrated by Perrin et al. [28]. A significant difference in BPA leaching among materials was observed, especial between C in relation to A and B (Fig. 7). The total BPA contented for material A was 5800 ppm ± 232, whereas material B and C leached 24% and 93% less BPA than material A, respectively.

No signal related to DCA was detected in any of the extractions with methanol. On the other hand, no BPA signal was observed for any

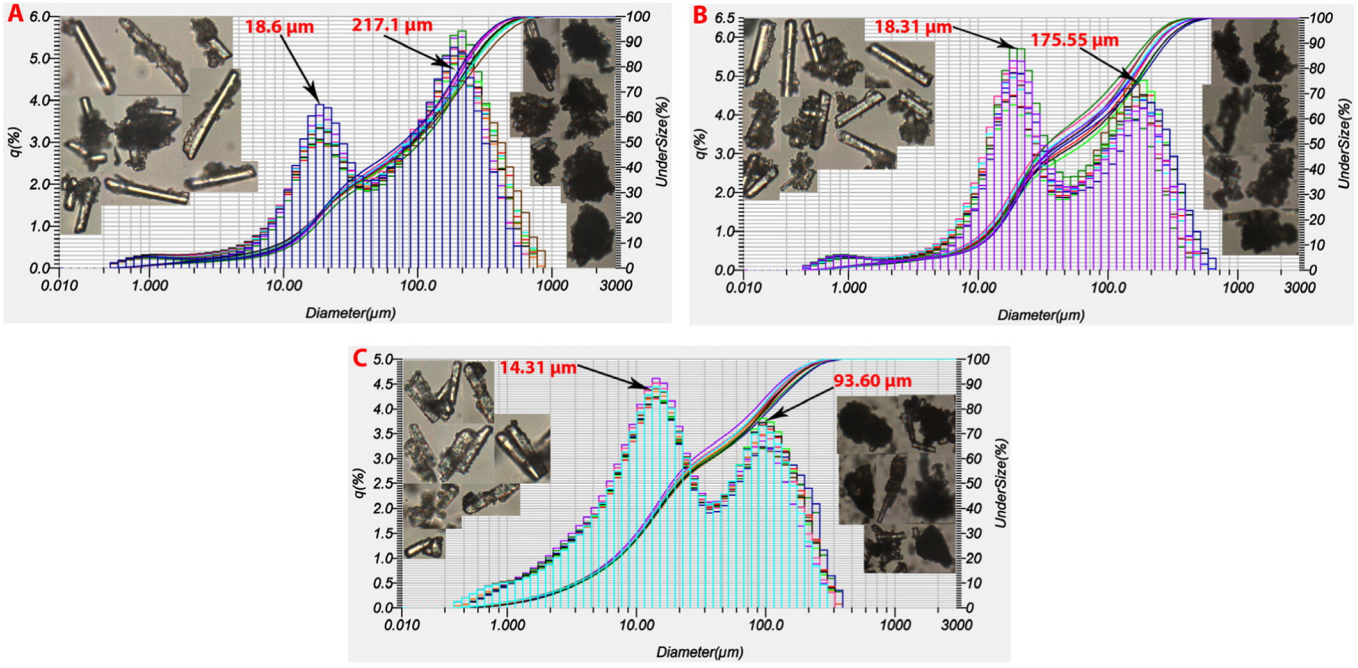

Fig. 3. Particle size distribution analysis of materials A, B and C by laser diffraction. Pictures were taken with 20× amplification lens for particles smeller than 50 μm and with 10× for bigger than 50 μm.

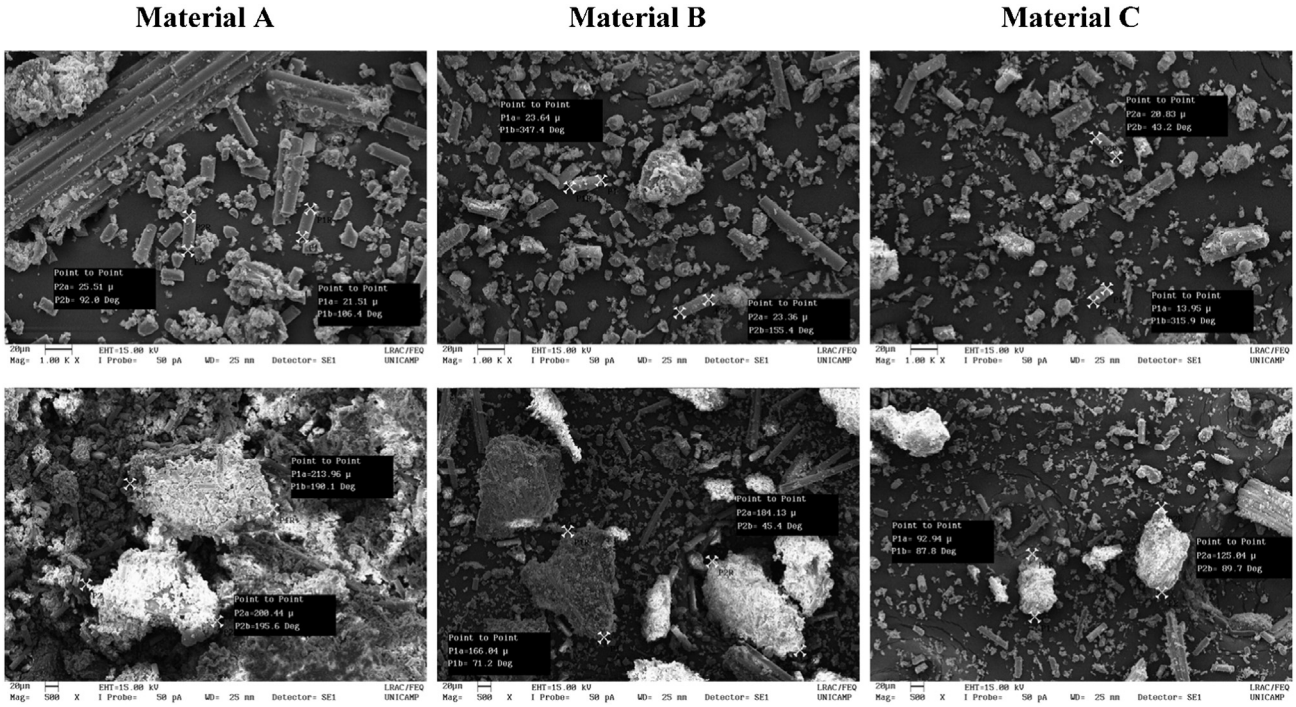

Fig. 4. SEM images of powered material A, B and C.

material in adsorption buffer experiments up to 28 days (Fig. 8). Material C showed the highest leaching of DCA, 838 ppm ± 72; followed by materials A and B with 213 ppm ± 35 and 187 ppm ± 72, respectively.

The attempted accelerated 56 days evaluation at 60 °C in adsorption buffer demonstrated that exposure of the material to a media that more closely resembles the human oral environment is capable of leaching both DCA and BPA in larger amounts relative to the other media. The results showed the presence of both BPA and DCA (Fig. 9). Material C presented the highest leaching rate, followed by materials A and B. Regarding DCA leaching in this accelerated leaching environment, material B showed the lowest amount, 666 ppm ± 95, of DCA, followed by material A with 1199 ppm ± 95, and then material C with 1680 ppm ± 96. The experiments demonstrate that there is an excess of crosslinking component in all materials, indicating the material formulation can be improved in order to reducing the excess of DCA initial composition.

BPA has a very high solubility in methanol (25 mg/mL), which is why it was used as solvent for the BPA total leaching determination. When the materials were submitted to a more clinically relevant medium, adsorption buffer, the highest leaching was found in material A (293 ppm) which represents 5% of the total leachable BPA in the sample. This is probably due to BPA's solubility in water (298 mg/L) suggesting that the medium was saturated and could no longer extract BPA from the material. The experiments were performed in batches while in the oral environment the saliva flows continuously. Even with a low flow, it would not be enough to saturate the medium, and eventually all leachable BPA present in the implanted material would be released in a long term exposure. A relevant point is the amount of BPA that could leach to the tissue which will be in contact with the implant. Due to polarity, the organic composition of the human tissue can extract more BPA than the saliva. For that, additional experiments must be conducted to evaluate material potential biocompatibility and applicability keeping in mind that recent bio-monitoring studies have suggested that human relevant exposures are higher than the currently proposed safe reference dose [36,37].

Considering that low molecular weight compounds are usually leached to the surrounding medium through direct contact and thus

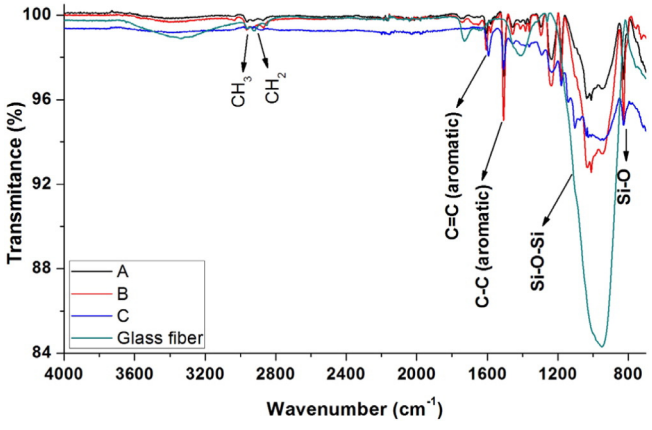

Fig. 5. FTIR Spectra of the samples A, B, C and glass fiber.

Table 4
Infrared absorption and Raman scattering assignment of bands for materials A, B and C.

Wavenumber (cm^{-1})	Bond	Infrared event	Raman event
823	Si–O	Si–OH – bending	Si–OH – bending
1000	Si–O	SiOSi – stretching	
1110	C–O		Aryl–O–alkyl – symmetric stretching
1140	C–O		Alkyl–O–alkyl – symetric stretching
1180	C–O	C–OH – stretching	C–OH – stretching
1240	C–O	ArylO–alkyl – asymmetric stretching	
1508	C–C	Aromatic – stretching	
1600	C=C	Aromatic – stretching	Aromatic – stretching
2926	C–H	CH_3 – stretching	CH_3 – stretching
2965	C–H	CH_2 – stretching	CH_2 – stretching
3060	C–H		Aromatic – stretching

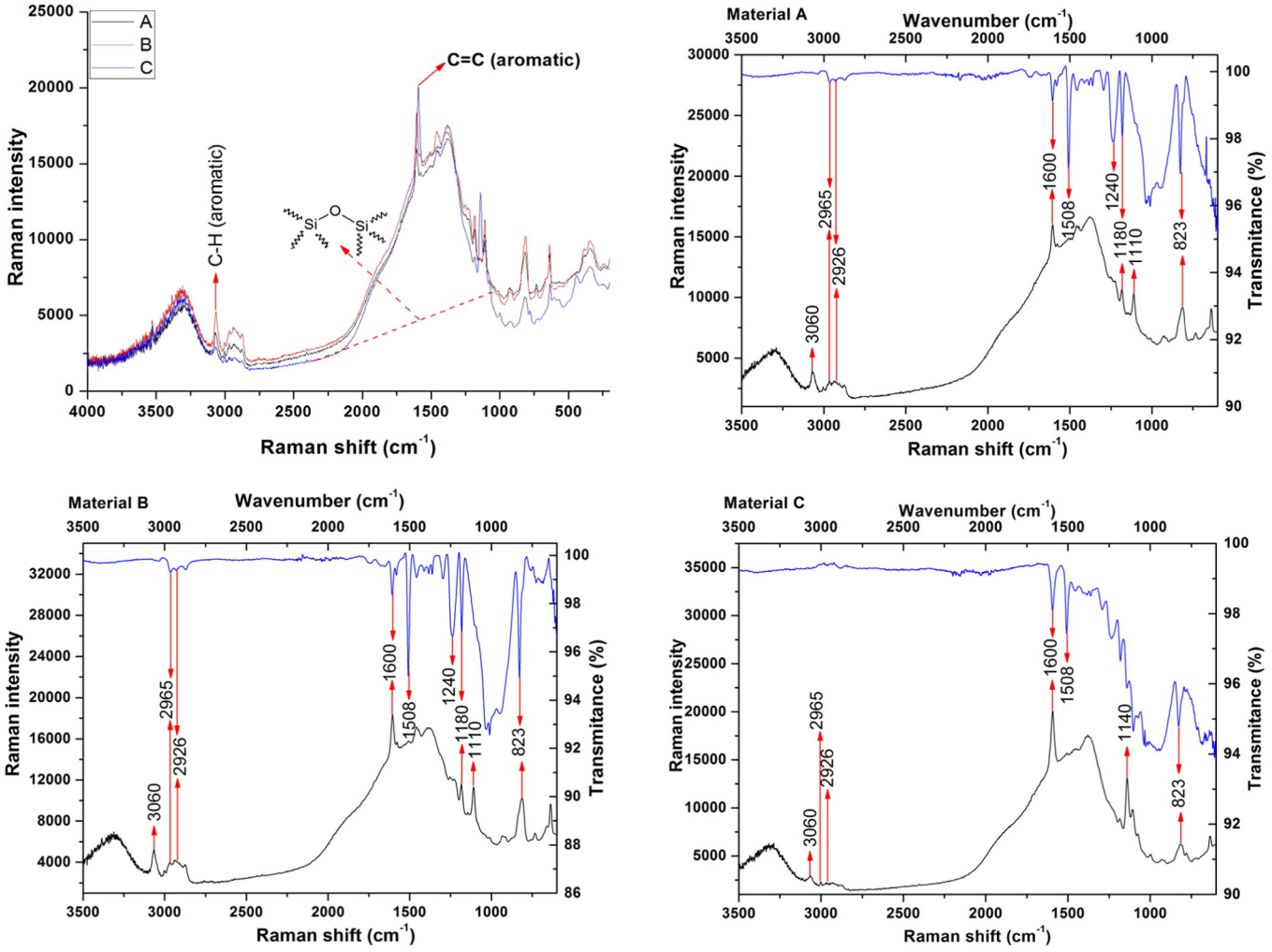

Fig. 6. Overlay of the Raman Spectra of the samples A, B and C; and the individual comparative Raman and FTIR spectra for the sample A, B and C.

its shape and form will play a significant role on the amounts detected. The detection observed when larger bulk samples were very low and thus milling was performed to accelerate experiments by increasing the material surface area. In order to determine the surface area of the powdered samples used to perform the leaching experiments, Brunauer–Emmett–Teller (BET) theory was used. We considered a molar crown made with materials A, B and C (each with surface area of 136 mm^2 [38])to estimate the total amount of BPA such a component size would leach. The data is summarized in the Table 5.

Our results show a dramatic decrease in the amount of BPA release when the chemical release was estimated as a function of an average molar crown surface area. The estimated release values, considering the adsorption buffer, shows the Material B would have the total

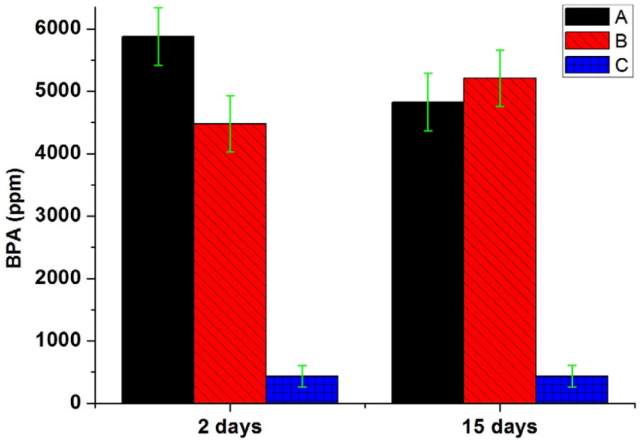

Fig. 7. BPA leaching in methanol at 25 °C after two days for samples A (5800 ppm ± 232), B (4482 ppm ± 226) and C (439 ppm ± 86); and 15 days for samples A (4825 ppm ± 232), B (5212 ppm ± 226) and C (441 ppm ± 86).

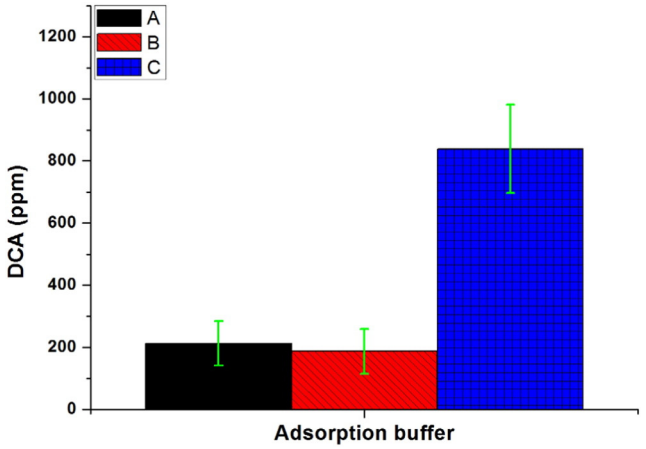

Fig. 8. DCA (ppm) leaching in adsorption buffer at 37 °C for 28 days of samples A (213 ppm ± 35), B (187 ppm ± 36) and C (838 ppm ± 72).

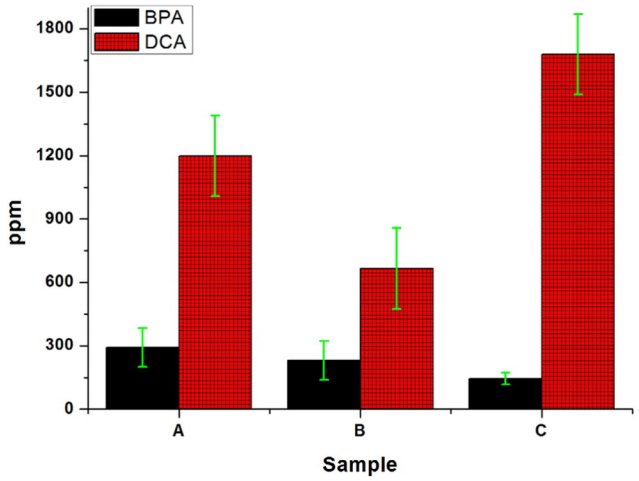

Fig. 9. BPA of the samples A (293 ppm ± 46), B (231 ppm ± 46) and C (145 ppm ± 14) and DCA of the samples A (1199 ppm ± 95), B (666 ppm ± 95) and C (1680 ppm ± 96) leaching in adsorption buffer at 60 °C for 56 days.

amount of 0.15 μg ± 0.03 of BPA, followed by the materials A and C with 0.14 μg ± 0.07 and 0.03 μg ± 0.003, respectively.

4. Conclusion

The design possibilities of fiber-reinforced composites are virtually limitless and for dental applications additional concerns regarding their esthetic output must be considered, which makes them an interesting alternative to replace metals. Whereas their composition can be tailored for the desired application, several parameters will orient their final indications in biomedical use such as strength (e.g. type of fiber, interfacial adhesion, etc.) and chemical stability considering its long-term interaction with host tissues and biofluids. Our physicochemical characterization was accomplished by several methods including FTIR, Raman, Brunauer-Emmett-Teller (BET) Analysis, X-ray fluorescence spectroscopy, and degradation experiments which revealed that the three provided materials A and B presented very similar chemical composition and glass fiber content, and material C belongs to a different class of BPA resin. The variations between them were more largely accounted by the different phase distribution than chemical composition. Specific biocompatibility testing should be conducted to determine if the differences herein detected might have clinical implications.

Acknowledgments

This work was partially supported by VJM Ltd. (Weck and Coelho). The authors thank Retsch Technology, specially Mr. Kyle James for his willingness to help us with cryomill; Horiba Scientific for Raman analyses, specially Mr. David Tuschel and Mr. Keith Swain for their precious help and advices, and Radchrom Analitica for assistance in the particle size analysis.

Appendix A. Supplementary data

Supplementary data to this article can be found online at http://dx.doi.org/10.1016/j.msec.2016.07.002.

References

[1] R. Mustafa, M.B.H. Othman, H. Ismail, Z. Ahmad, Synthesis and characterization of rigid aromatic-based epoxy resi, Malays. Polym. J. 6 (2011) 68–75.
[2] A. Cherdoud-Chihani, M. Mouzali, M.J.M. Abadie, Etude de la reticulation DGEBA-poly(styrène-alt-anhydride maléique) par DSC isotherme, Eur. Polym. J. 33 (1997) 1415–1422.
[3] O. Zabihi, A. Khodabandeh, S. Ghasemlou, Investigation of mechanical properties and cure behavior of DGEBA/nano-Fe_2O_3 with polyamine dendrimer, Polym. Degrad. Stab. 97 (2012) 1730–1736.
[4] S. Zheng, Nanostructured Epoxies by the Use of Block Copolymers, Epoxy Polymers, Wiley-VCH Verlag GmbH & Co. KGaA, 2010 79–108.
[5] J.-P. Pascault, R.J.J. Williams, General Concepts about Epoxy Polymers, Epoxy Polymers, Wiley-VCH Verlag GmbH & Co. KGaA, 2010 1–12.
[6] S. Paz Abuín, Epoxy Adhesives: A View of the Present and the Future, Epoxy Polymers, Wiley-VCH Verlag GmbH & Co. KGaA, 2010 213–234.
[7] Z. Fan, F. Gong, S.T. Nguyen, H.M. Duong, Advanced multifunctional graphene aerogel–poly (methyl methacrylate) composites: experiments and modeling, Carbon 81 (2015) 396–404.
[8] M. Hassan, K.R. Reddy, E. Haque, A.I. Minett, V.G. Gomes, High-yield aqueous phase exfoliation of graphene for facile nanocomposite synthesis via emulsion polymerization, J. Colloid Interface Sci. 410 (2013) 43–51.
[9] S.J. Han, H.-I. Lee, H.M. Jeong, B.K. Kim, A.V. Raghu, K.R. Reddy, Graphene modified lipophilically by stearic acid and its composite with low density polyethylene, J. Macromol. Sci., Part B 53 (2014) 1193–1204.
[10] K.R. Reddy, K.P. Lee, A.I. Gopalan, A.M. Showkat, Synthesis and properties of magnetite/poly (aniline-co-8-amino-2-naphthalenesulfonic acid)(SPAN) nanocomposites, Polym. Adv. Technol. 18 (2007) 38–43.
[11] K.R. Reddy, M. Hassan, V.G. Gomes, Hybrid nanostructures based on titanium dioxide for enhanced photocatalysis, Appl. Catal. A Gen. 489 (2015) 1–16.
[12] A. Gloria, D. Ronca, T. Russo, U. D'Amora, M. Chierchia, R. De Santis, L. Nicolais, L. Ambrosio, Technical features and criteria in designing fiber-reinforced composite materials: from the aerospace and aeronautical field to biomedical applications, J. Appl. Biomater. Biomech.: JABB 9 (2011) 151–163.
[13] J. Juloski, G.M. Fadda, F. Monticelli, M. Fajo-Pascual, C. Goracci, M. Ferrari, Four-year survival of endodontically treated premolars restored with fiber posts, J. Dent. Res. 93 (2014) 52S–58S.
[14] M. Ferrari, M.C. Cagidiaco, S. Grandini, M. De Sanctis, C. Goracci, Post placement affects survival of endodontically treated premolars, J. Dent. Res. 86 (2007) 729–734.
[15] E. Erkmen, G. Meric, A. Kurt, Y. Tunc, A. Eser, Biomechanical comparison of implant retained fixed partial dentures with fiber reinforced composite versus conventional metal frameworks: a 3D FEA study, J. Mech. Behav. Biomed. Mater. 4 (2011) 107–116.
[16] J.E. Cooper, E.L. Kendig, S.M. Belcher, Assessment of bisphenol a released from reusable plastic, aluminium and stainless steel water bottles, Chemosphere 85 (2011) 943–947.
[17] R. Rezg, S. El-Fazaa, N. Gharbi, B. Mornagui, Bisphenol a and human chronic diseases: current evidences, possible mechanisms, and future perspectives, Environ. Int. 64 (2014) 83–90.
[18] T. Geens, D. Aerts, C. Berthot, J.-P. Bourguignon, L. Goeyens, P. Lecomte, G. Maghuin-Rogister, A.-M. Pironnet, L. Pussemier, M.-L. Scippo, J. Van Loco, A. Covaci, A review of dietary and non-dietary exposure to bisphenol-A, Food Chem. Toxicol. 50 (2012) 3725–3740.
[19] D. Kloukos, N. Pandis, T. Eliades, In vivo bisphenol-A release from dental pit and fissure sealants: a systematic review, J. Dent. 41 (2013) 659–667.
[20] A. Kingman, J. Hyman, S.A. Masten, B. Jayaram, C. Smith, F. Eichmiller, M.C. Arnold, P.A. Wong, J.M. Schaeffer, S. Solanki, W.J. Dunn, Bisphenol a and other compounds in human saliva and urine associated with the placement of composite restorations, J. Am. Dent. Assoc. 143 (2012) 1292–1302.
[21] A.M. Calafat, Urinary concentrations of bisphenol A and 4-nonylphenol in a human reference population, Environ. Health Perspect. 113 (2005) 391–395.
[22] S. Ehrlich, P.L. Williams, R. Hauser, S.A. Missmer, J. Peretz, A.M. Calafat, J.A. Flaws, Urinary bisphenol A concentrations and cytochrome P450 19 A1 (Cyp19) gene expression in ovarian granulosa cells: an in vivo human study, Reprod. Toxicol. 42 (2013) 18–23.

Table 5
BPA leaching in relation with surface area.

Material	Powder material					Molar Crown	
	Surface Area	Total BPA		BPA (adsorption buffer)		Total BPA	BPA (adsorption buffer)
	mm^2/g	ppm	$\mu g_{BPA}/mm^2$	ppm	$\mu g_{BPA}/mm^2$	μg_{BPA}	μg_{BPA}
A	2.95×10^{-5}	5880	0.020	293	0.0010	2.71 ± 0.3	0.14 ± 0.03
B	2.06×10^{-5}	4482	0.022	231	0.0011	2.96 ± 0.3	0.15 ± 0.07
C	7.73×10^{-5}	439	0.001	145	0.0002	0.08 ± 0.008	0.03 ± 0.003

[23] H.I. Zeliger, Exposure to lipophilic chemicals as a cause of neurological impairments, neurodevelopmental disorders and neurodegenerative diseases, Interdiscip. Toxicol. 6 (2013) 103–110.
[24] J.D. Meeker, Exposure to environmental endocrine disrupting compounds and men's health, Maturitas 66 (2010) 236–241.
[25] A.F. Fleisch, P.E. Sheffield, C. Chinn, B.L. Edelstein, P.J. Landrigan, Bisphenol A and related compounds in dental materials, Pediatrics 126 (2010) 760–768.
[26] S. Duarte, S. Gregoire, A.P. Singh, N. Vorsa, K. Schaich, W.H. Bowen, H. Koo, Inhibitory effects of cranberry polyphenols on formation and acidogenicity of *Streptococcus mutans* biofilms, FEMS Microbiol. Lett. 257 (2006) 50–56.
[27] S. Duarte, H. Koo, W.H. Bowen, M.F. Hayacibara, J.A. Cury, M. Ikegaki, P.L. Rosalen, Effect of a novel type of propolis and its chemical fractions on glucosyltransferases and on growth and adherence of *Mutans Streptococci*, Biol. Pharm. Bull. 26 (2003) 527–531.
[28] F.X. Perrin, T.M.H. Nguyen, T.M.L. Tran, J.L. Vernet, Determination of bisphenol A (BPA) by gas chromatography–mass spectrometry and ^{1}H NMR spectroscopy during curing of epoxy–amine resins, Polym. Test. 25 (2006) 912–922.
[29] F.T. Wallenberger, R.J. Hicks, A.T. Bierhals, Design of environmentally friendly fiberglass compositions: ternary eutectic SiO_2–Al_2O_3–CaO compositions, structures and properties, J. Non-Cryst. Solids 349 (2004) 377–387.
[30] W. Gao, Z. Li, N.M. Sammes, An Introduction to Electronic Materials for Engineers, World Scientific, Singapore, Hackensack, NJ, 2011.
[31] J. Leitner, M. Nevřiva, D. Sedmidubský, P. Voňka, Enthalpy of formation of selected mixed oxides in a CaO–SrO–Bi_2O_3–Nb_2O_5 system, J. Alloys Compd. 509 (2011) 4940–4943.
[32] K. Singh, H. Singh, G. Sharma, L. Gerward, A. Khanna, R. Kumar, R. Nathuram, H.S. Sahota, Gamma-ray shielding properties of CaO–SrO–B_2O_3 glasses, Radiat. Phys. Chem. 72 (2005) 225–228.
[33] A.J. Bonon, Y.N. Kozlov, J.O. Bahú, R.M. Filho, D. Mandelli, G.B. Shul'pin, Limonene epoxidation with H_2O_2 promoted by Al_2O_3: kinetic study, experimental design, J. Catal. 319 (2014) 71–86.
[34] N. Sheppard, C. De La Cruz, Vibrational spectra of hydrocarbons adsorbed on metals: Part II. Adsorbed acyclic alkynes and alkanes, cyclic hydrocarbons including aromatics, and surface hydrocarbon groups derived from the decomposition of alkyl halides, etc. in: W.O.H.B.G.D.D. Eley, K. Helmut (Eds.), Advances in Catalysis, Academic Press 1998, pp. 181–313.
[35] D.D. Seachrist, K.W. Bonk, S.M. Ho, G.S. Prins, A.M. Soto, R.A. Keri, A review of the carcinogenic potential of bisphenol A, Reprod. Toxicol. (2015), http://dx.doi.org/10.1016/j.reprotox.2015.09.006.
[36] F.S.v. Saal, W.V. Welshons, Evidence that bisphenol A (BPA) can be accurately measured without contamination in human serum and urine, and that BPA causes numerous hazards from multiple routes of exposure, Mol. Cell. Endocrinol. 398 (2014) 101–113.
[37] L.N. Vandenberg, I. Chahoud, V. Padmanabhan, F.J. Paumgartten, G. Schoenfelder, Biomonitoring studies should be used by regulatory agencies to assess human exposure levels and safety of bisphenol A, Environ. Health Perspect. 118 (2010) 1051–1054.
[38] D.C.N. Chan, B.H.W. Chan, A.K.H. Chung, Mathematical modeling of molar tooth preparations for complete crowns, J. Dent. 35 (2007) 875–877.

Physicochemical Characterization of Three Fiber-Reinforced Epoxide-Based Composites for Dental Applications

Anderson J. Bonon[a], Marcus Weck[b], Estevam A. Bonfante[c]*, Paulo G. Coelho[d,e,f]

[a] Faculdade de Engenharia Química, Universidade Estadual de Campinas, Av. Albert Einstein, 500, Campinas – SP, CEP 13083-852, Brazil
[b] Molecular Design Institute and Department of Chemistry, New York University, New York, NY 10003, United States
[c] Department of Prosthodontics, University of Sao Paulo - Bauru School of Dentistry, Bauru, Brazil
[d]Department of Biomaterials and Biomimetics, New York University College of Dentistry, New York, NY, USA
[e] Director for Research, Department of Periodontology and Implant Dentistry, New York University College of Dentistry, New York, NY, USA
[f] Affiliated Faculty, Department of Engineering, New York University Abu Dhabi, Abu Dhabi, United Arab Emirates

*Corresponding author

Estevam A. Bonfante, estevamab@gmail.com

Department of Prosthodontics, University of São Paulo, Al Otávio Pinheiro Brisola 9-75, Bauru, SP, Brazil, 17.012-901. Phone +55 (14) 3235-8277

Supplementary material

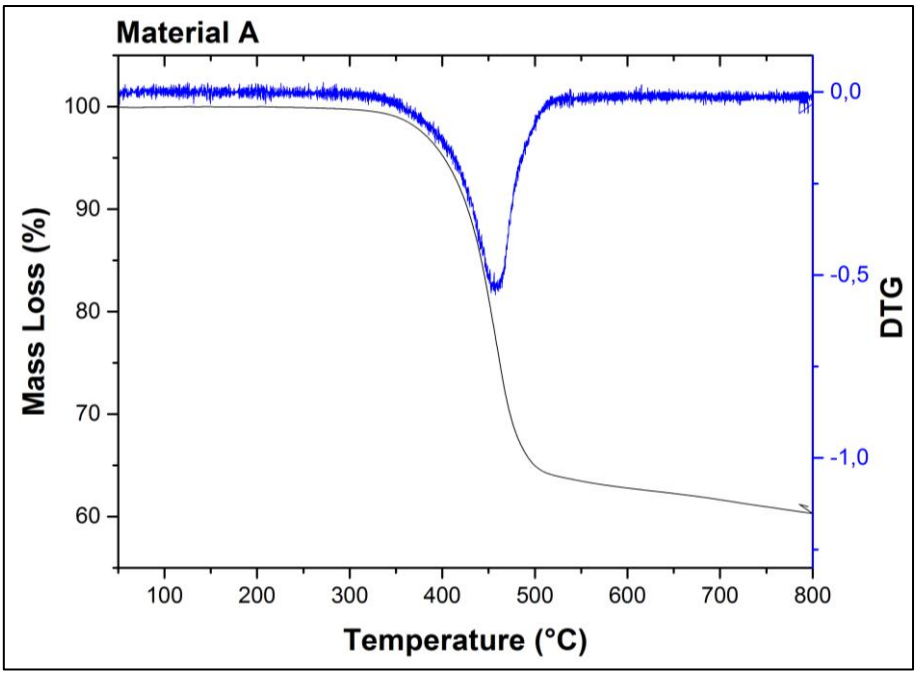
Material A
Mass Loss (%)
100
90
80
70
60
100
200
300
400
500
600
700
800
Temperature (°C)
0,0
-0,5
-1,0
DTG

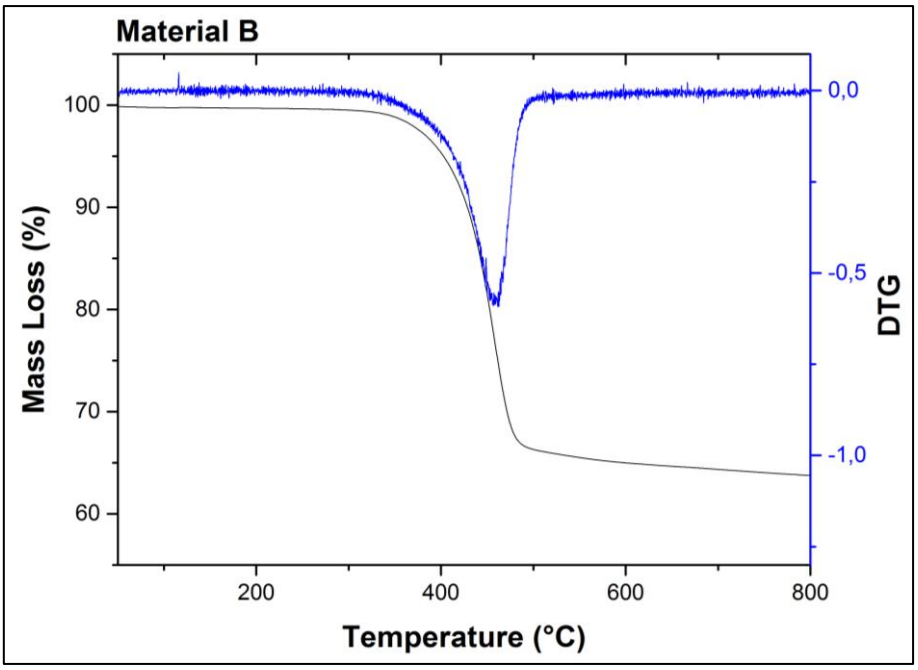
Material B
Mass Loss (%)
100
90
80
70
60
200
400
600
800
Temperature (°C)
0,0
-0,5
-1,0
DTG

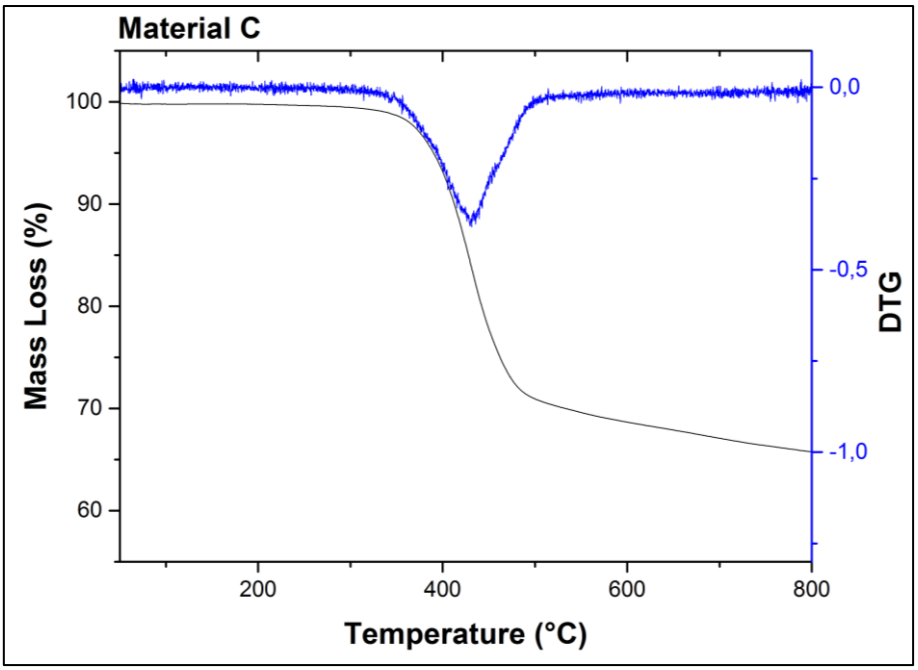

Figure S1: Thermogram with the respective derivative thermos-gravimetric (DTG) of the samples A, B and C. The displaced data are average of triplicate measurements.

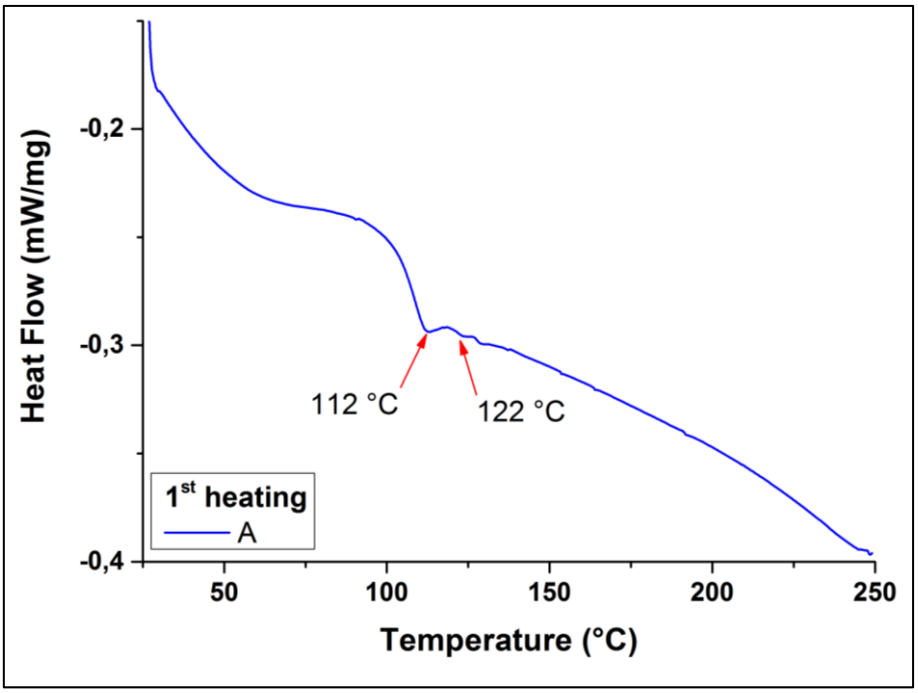

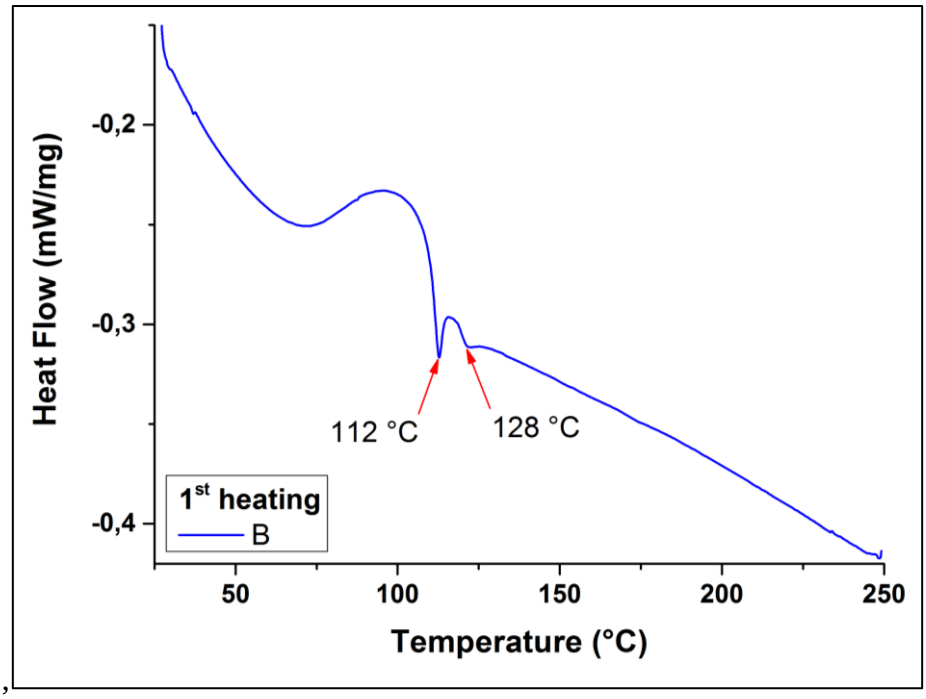

,

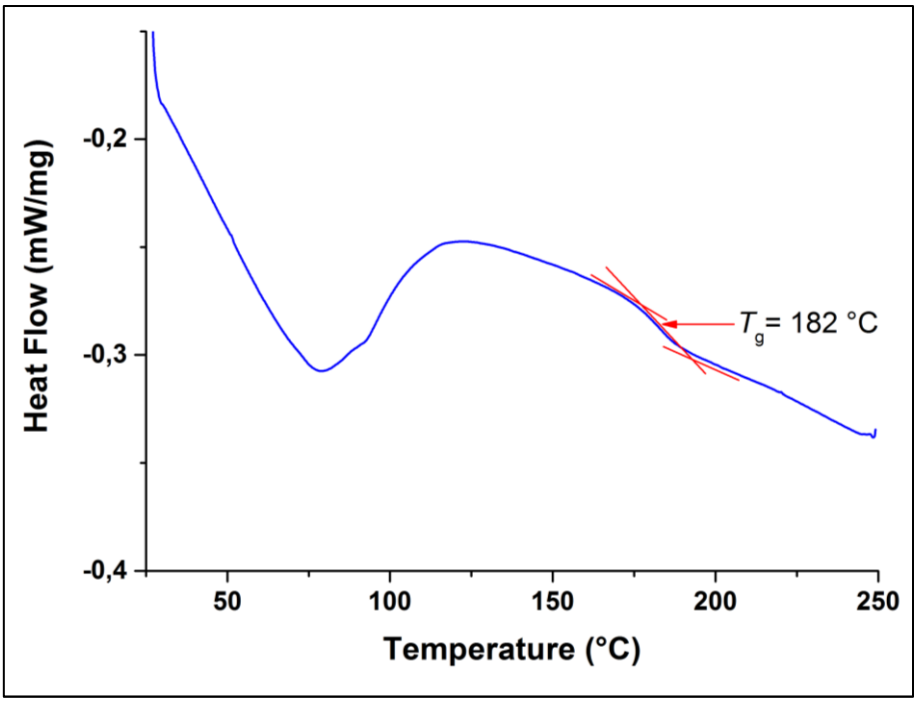

Figure S2: Thermogram with the DSC for the first heating of the samples A, B and C.

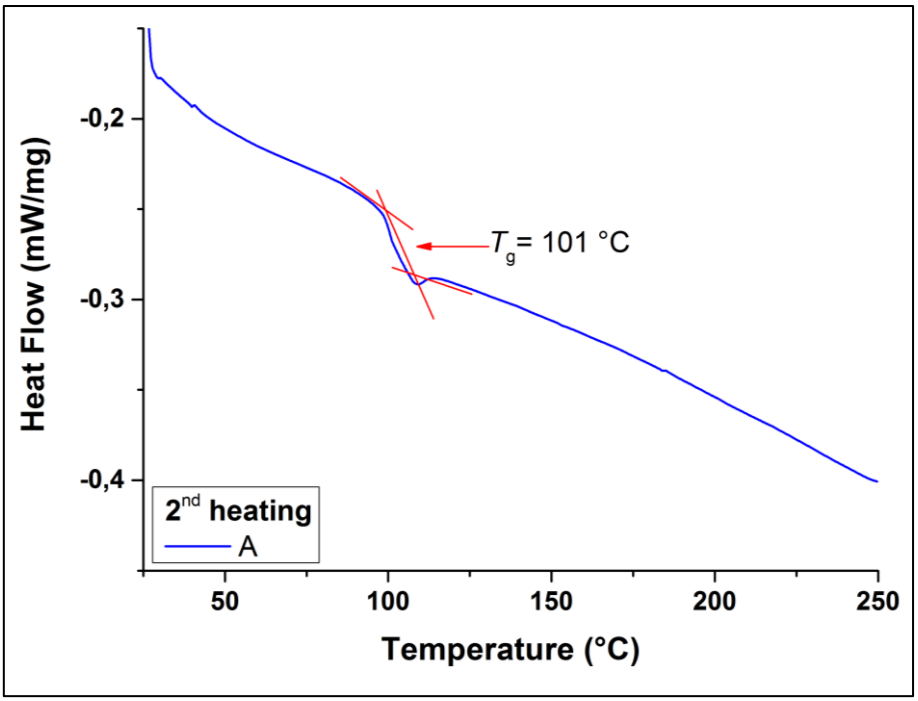
Heat Flow (mW/mg)
-0,2
-0,3
-0,4
T_g= 101 °C
2nd heating
A
50
100
150
200
250
Temperature (°C)

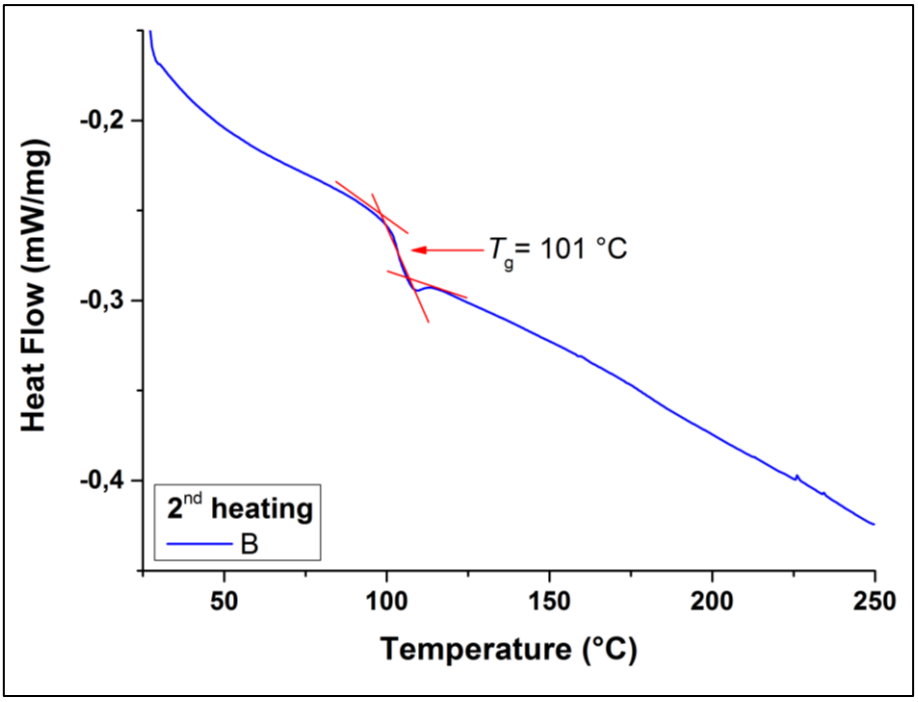
Heat Flow (mW/mg)
-0,2
-0,3
-0,4
T_g= 101 °C
2nd heating
B
50
100
150
200
250
Temperature (°C)

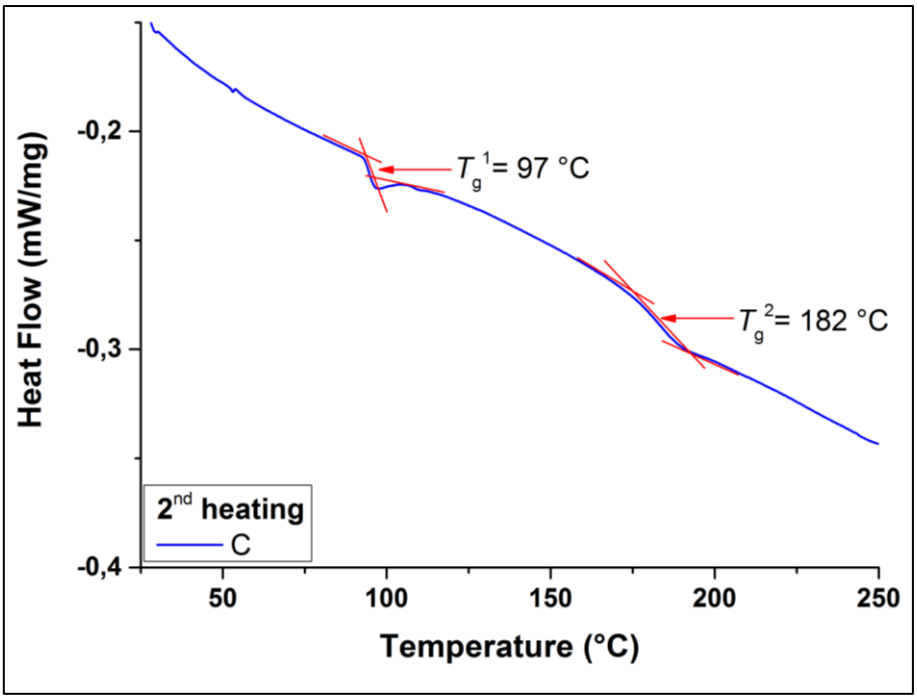

Figure S3: Thermogram with the DSC for the second heating of the samples A, B and C.

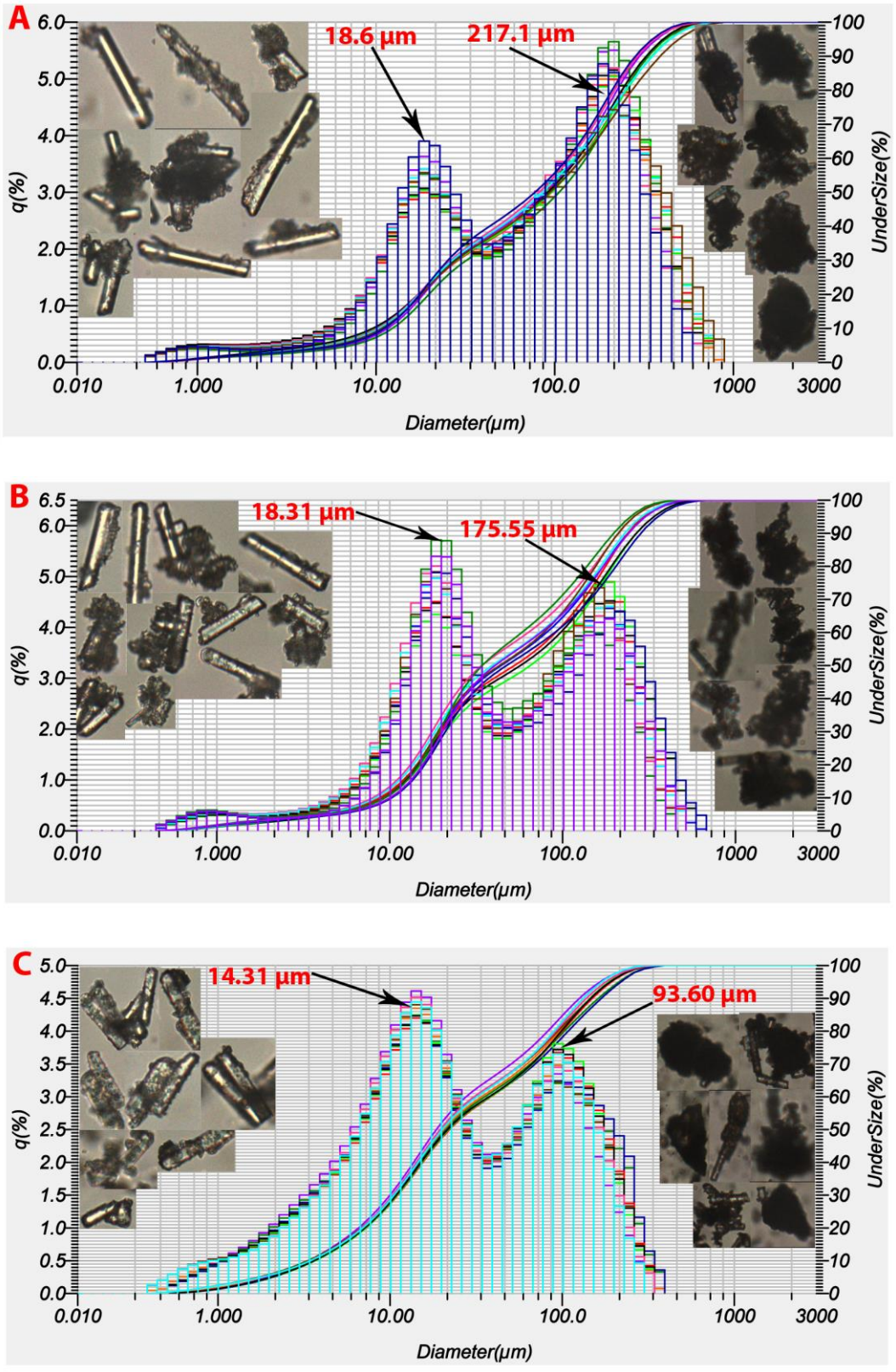

Figure S4: Particle size distribution analysis of Materials A, B and C by laser diffraction. Pictures were taken with 20X amplification lens for particles smeller than 50µm and with 10X for bigger than 50 µm.

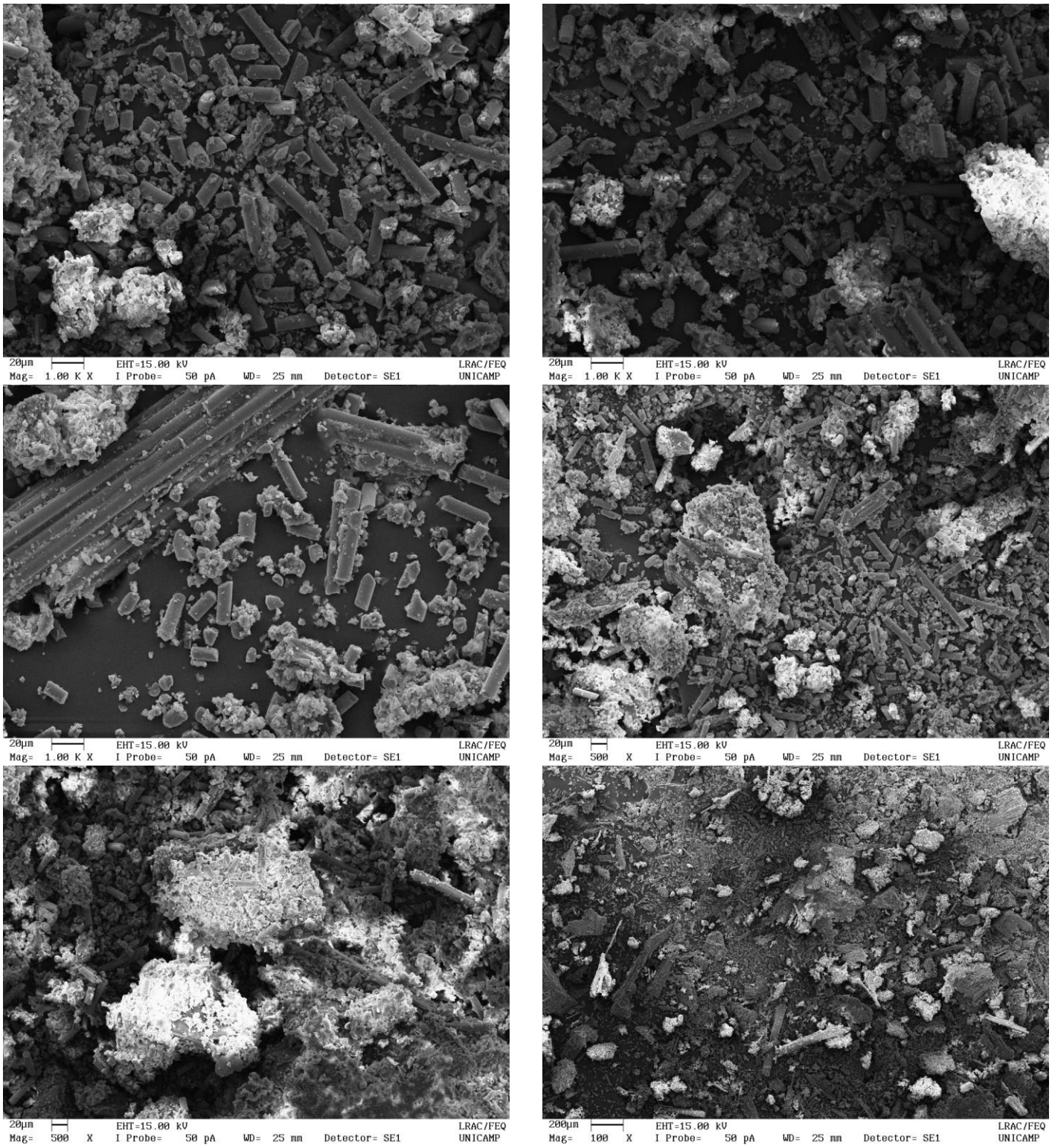

Figure S5: SEM of Material A

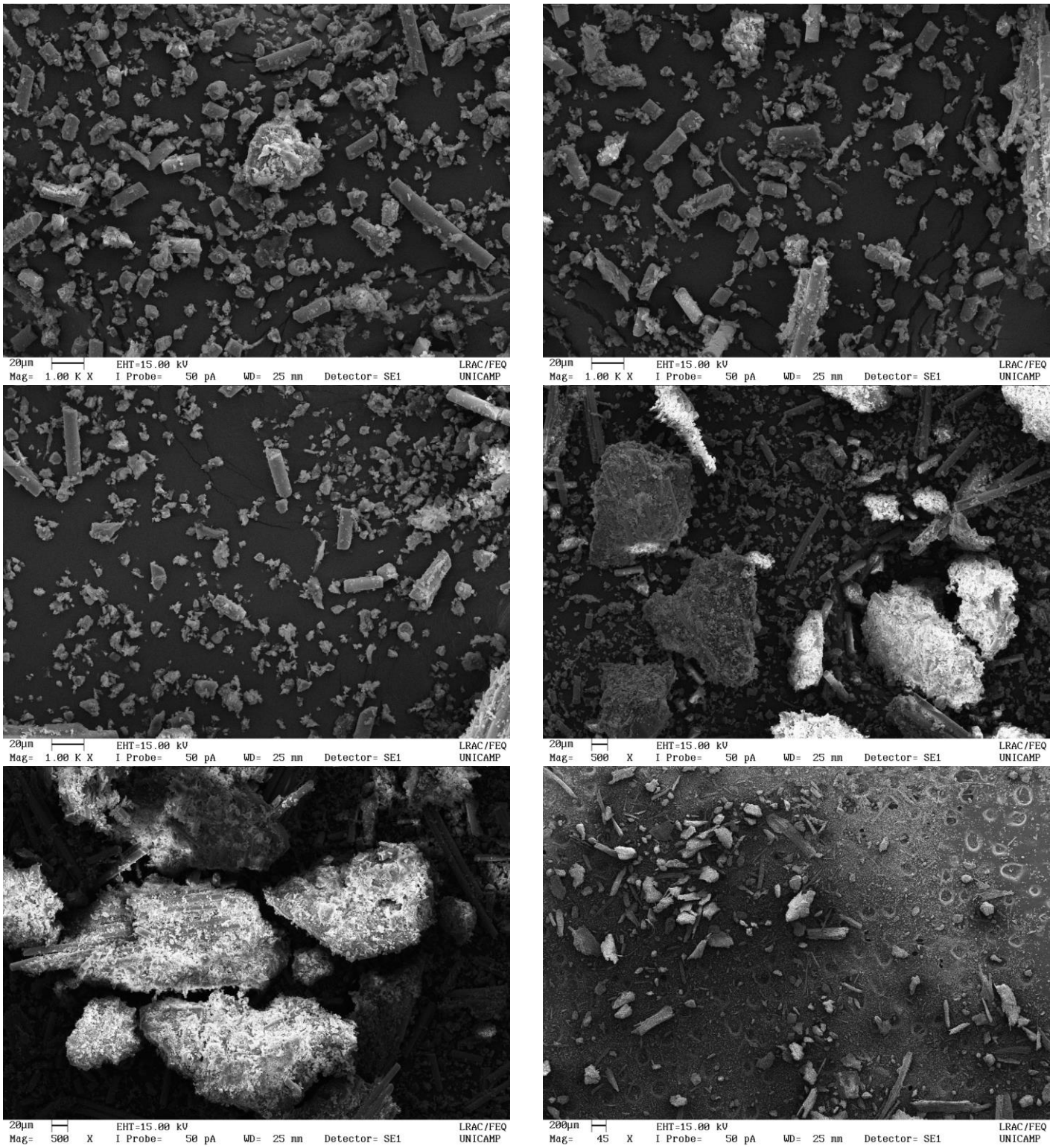

Figure S6: SEM of Material B

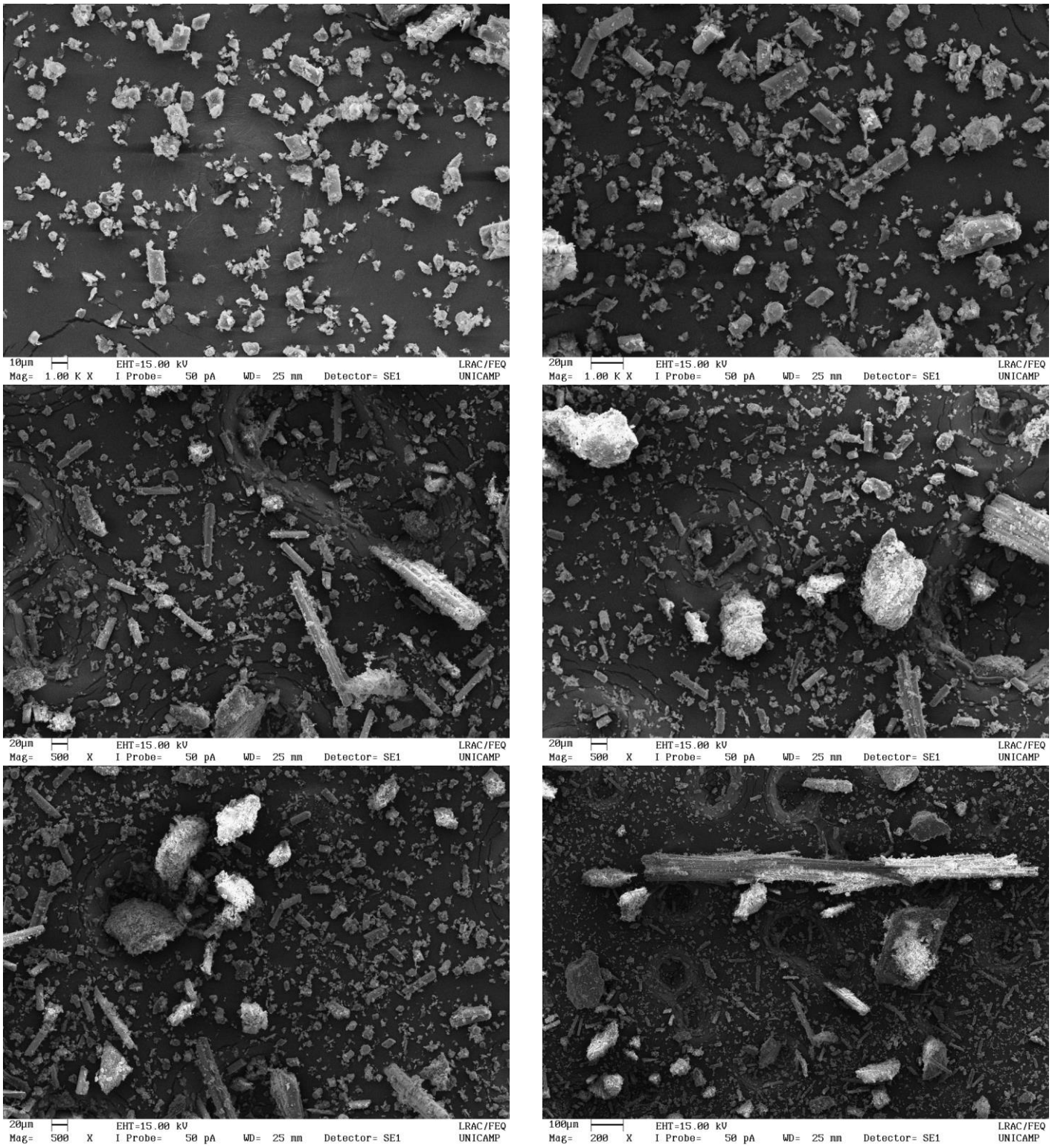

Figure S7: SEM of Material C.

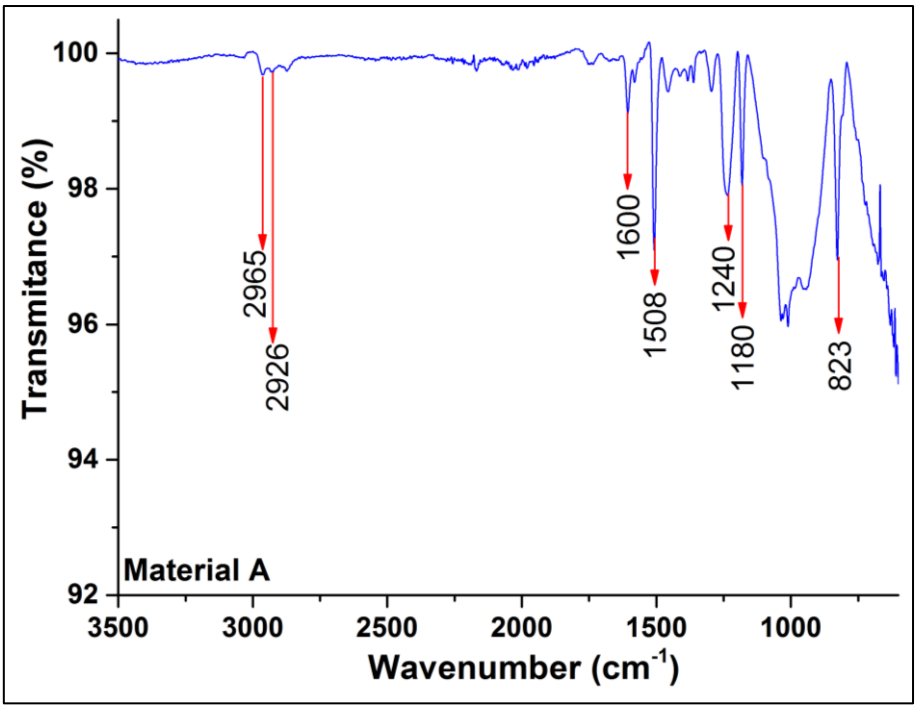
Transmitance (%)
100
98
96
94
92
2965
2926
1600
1508
1240
1180
823
Material A
3500
3000
2500
2000
1500
1000
Wavenumber (cm-1)

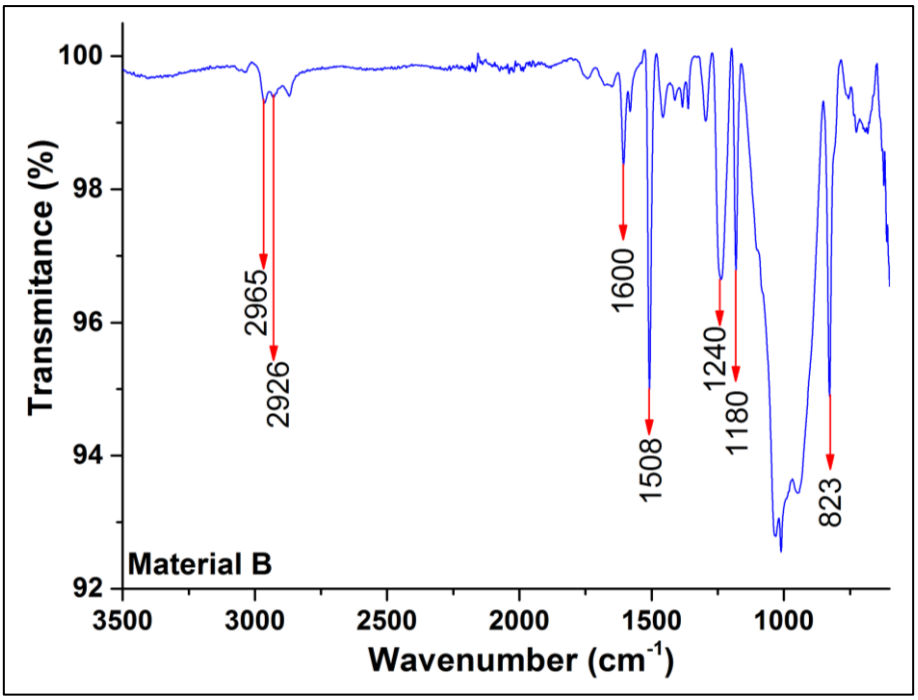
Transmitance (%)
100
98
96
94
92
2965
2926
1600
1508
1240
1180
823
Material B
3500
3000
2500
2000
1500
1000
Wavenumber (cm-1)

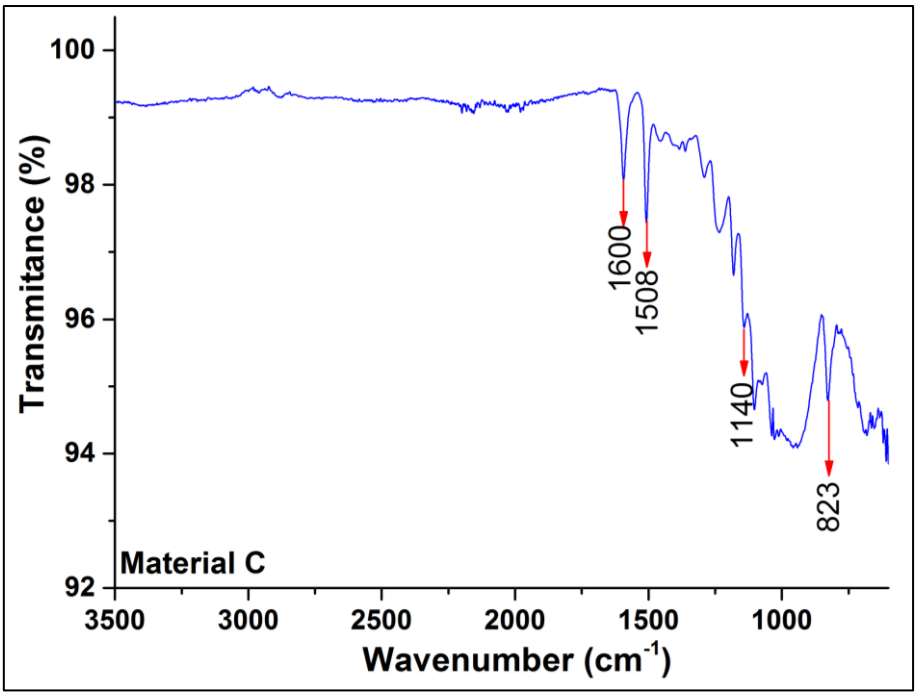

Figure S8: FTIR spectrum of the samples A, B and C.

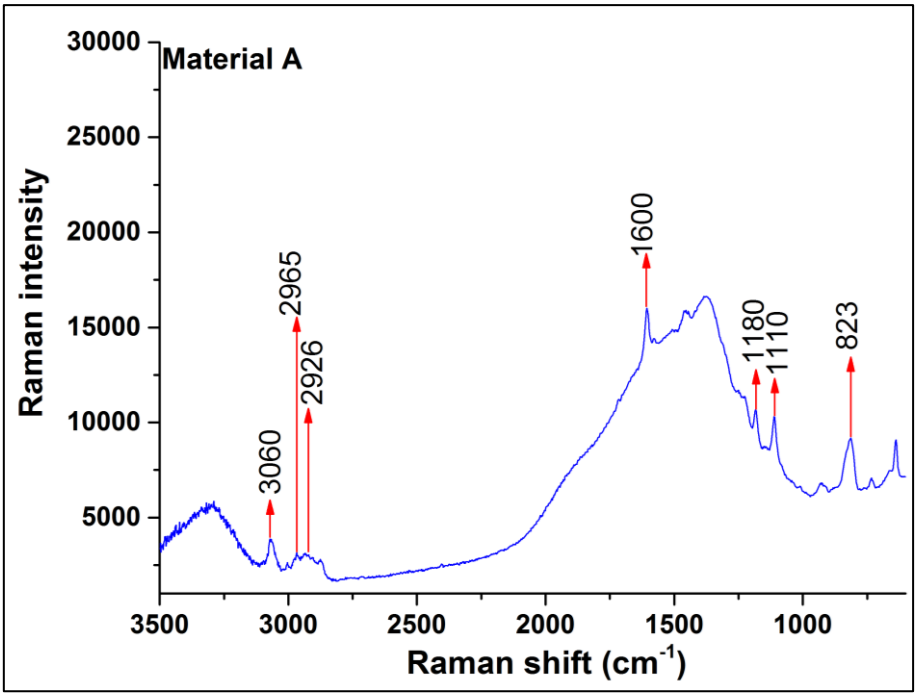

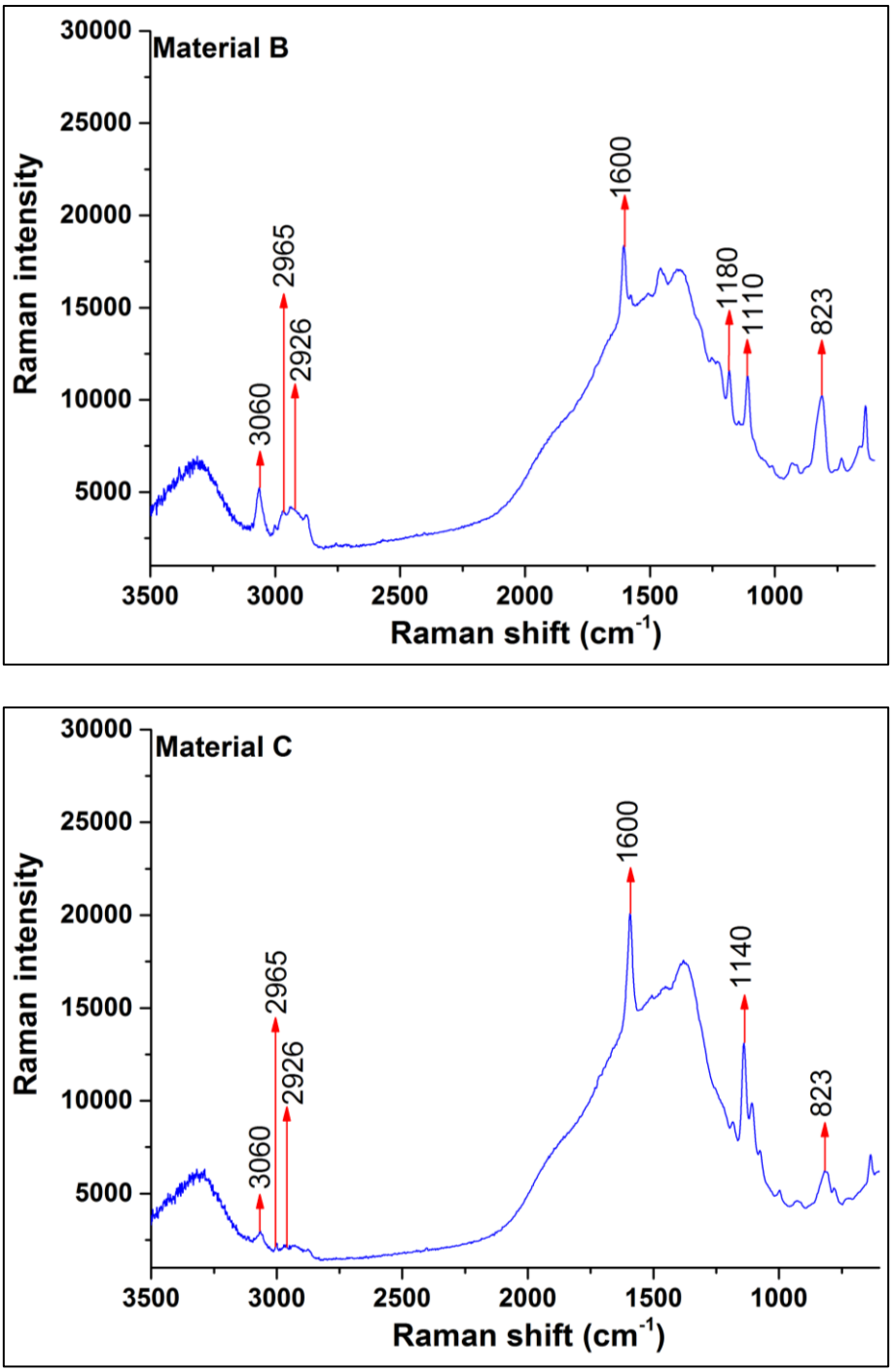

Figure S9: FT-Raman spectrum of the samples A, B and C.

Table S1: Infrared absorption and Raman scattering assignment of the ban for materials A, B and C.

Wavenumber (cm^{-1})	Bond	Infrared Event	Raman Event
823	Si–O	Si-OH – bending	Si-OH – bending
1000	Si–O	Si-O-Si – stretching	
1110	C–O		Aryl-O-alkyl – symmetric stretching
1140	C–O		Alkyl-O-alkyl – stretching
1180	C–O	C-OH – stretching	C-OH – stretching
1240	C–O	Aryl-O-alkyl – asymmetric stretching	
1508	C–C	aromatic – stretching	
1600	C=C	aromatic – stretching	aromatic – stretching
2926	C–H	CH_3 – stretching	CH_3 – stretching
2965	C–H	CH_2 – stretching	CH_2 – stretching
3060	C–H		aromatic – stretching

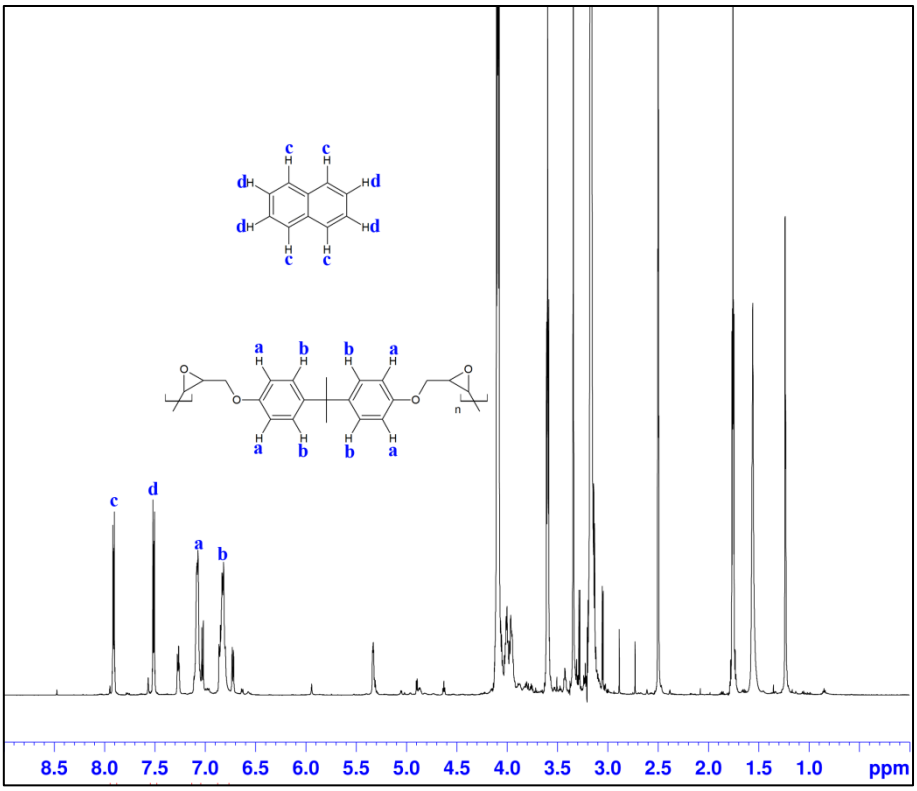

Figure S10: Typical ^{1}H RMN spectrum of BPA leaching experiment in methanol, using naphthalene as internal stander for quantification.

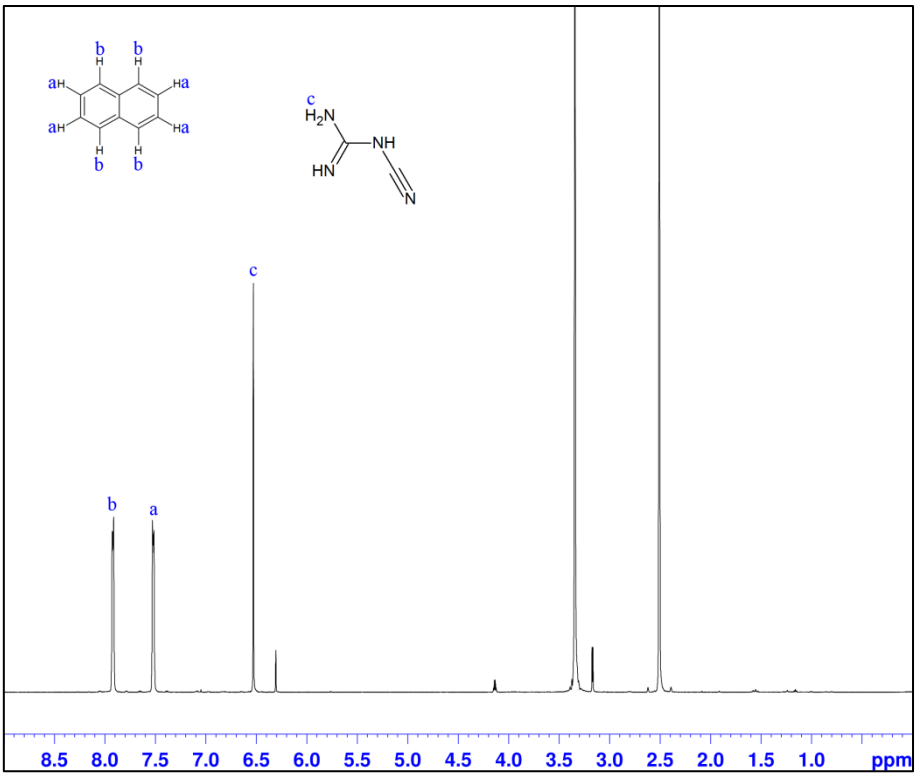

Figure S11: Typical ^{1}H RMN spectrum of DCA leaching experiment in adsorption buffer, using naphthalene as internal stander for quantification.